AN ABSTRACT OF THE THESIS OF

JAMES LEO HURLEY (Name) for the MASTER OF SCIENCE (Degree)

in Nuclear Engineering (Major) presented on May 1, 1970 (Date)

Title: DESIGN AND CALIBRATION OF A DEEP OCEAN NUCLEAR MOISTURE METER

Redacted for Privacy

Abstract approved: John C. Ringle

A prototype deep ocean nuclear moisture meter was developed based on the detection of epithermal neutrons backscattered from marine sediment molecules. Development consisted of choosing a source, a detector, containment materials, and associated counting equipment, followed by the construction and calibration of the probe. Thermal neutron response of the probe under various configurations was also studied. Moisture meter performance was predicted by a one-dimensional neutron diffusion code and the results compared with experimental measurements. It was found that a deep ocean probe could be built whose output was not affected by the type and quantities of solids found in a marine environment.

Design and Calibration of a Deep Ocean Nuclear Moisture Meter

by

James Leo Hurley

A THESIS

submitted to

Oregon State University

in partial fulfillment of
the requirements for the
degree of

Master of Science

June 1970

APPROVED:

Redacted for Privacy

Associate Professor of Mechanical and Nuclear Engineering

in charge of major

Redacted for Privacy

Head of Department of Mechanical and Nuclear Engineering

Redacted for Privacy

Dean of Graduate School

Date thesis is presented May 1, 1970

Typed by Nancy Kerley for James Leo Hurley

ACKNOWLEDGEMENT

The work described herein was performed as part of research done under a contract from the U. S. Naval Civil Engineering Laboratory, Port Hueneme, California (Contract No. N62-399-69-C-0009).

The author wishes to thank Drs. J. C. Ringle and J. R. Bell for their helpful suggestions and criticisms, and Max Clausen for his invaluable technical aid. Special thanks are extended to the author's wife for her endless patience, encouragement, and assistance, and to Sean Hurley for his inspiration and the use of his name.

TABLE OF CONTENTS

		Page
I.	INTRODUCTION AND BACKGROUND	1
II.	GENERAL NEUTRON MOISTURE INSTRUMENT THEORY	5
III.	NEUTRON SOURCES	31
IV.	DETECTORS AND ASSOCIATED EQUIPMENT	34
V.	EXPERIMENTAL MEASUREMENTS	39
VI.	EXPERIMENTAL PROCEDURES	58
VII.	GENERAL DISCUSSION	64
VIII.	CONCLUSIONS AND DESIGN SPECIFICATIONS	79
	BIBLIOGRAPHY	81
	APPENDICES	82

LIST OF TABLES

Table		Page
1	Group Structure for Multigroup Solutions.	18
2	Equipment.	40
3	Analysis of Soil Constituents.	43
4	Effect of Container Material on Instrument Response.	52
5	Epithermal Neutron Counting Data.	70
6	Thermal Neutron Counting Data.	72
7	Comparison of Moisture Content Measurements.	77

LIST OF FIGURES

Figure		Page
1	Variation in Thermal and Epithermal Neutron Flux in Water with Variation in Boron Concentration.	20
2	Variation of Thermal and Epithermal Neutron Flux in Water with Variation in Chlorine Concentration.	21
3	Front View of Moisture Meter Neutron Counting Equipment.	44
4	Side View of Moisture Test Stand.	44
5a	Top View of Test Stand.	45
5b	Top View of Detector Entering Zircaloy Pipe.	45
6a	Side View of Detectors and Source Holder.	46
6b	End View of Detectors and Source Holder, Detector End Plate Not Attached.	46
7	Output Spectrum of $Li^6I(Eu)$ Detector in Fresh Water.	47
8	Output Spectrum of Gd Detector in Fresh Water.	48
9	Variation of Epithermal Neutron Count Rate with Source-Detector Distance for LiI Detector (Cd Covered) in Zircaloy-2 Pipe.	49
10	Variation of Thermal Neutron Count Rate with Source-Detector Distance for LiI Detector (Bare) in Zircaloy-2 Pipe.	50
11	Variation in Count Rate with Temperature for LiI Instrument in Tap Water for Thermal and Epithermal Flux.	53
12	Epithermal Neutron Response of LiI Instrument.	54
13	Thermal Neutron Response of LiI Instrument.	55
14	Thermal Neutron Response of BF_3 Instrument.	56

LIST OF FIGURES (continued)

Figure		Page
15	Response of Gd Loaded Instrument.	57
16	Block Diagram of Instrument Operating and Test Circuits.	61

DESIGN AND CALIBRATION OF A DEEP OCEAN NUCLEAR MOISTURE METER

I. INTRODUCTION AND BACKGROUND

This research was sponsored by the U. S. Naval Civil Engineering Laboratory with the intent of having a nuclear moisture meter developed which could be used either alone or with a nuclear density meter to determine moisture content in the ocean floor with a minimum number of marine sediment samples.

The attempts to fulfill this intent encompassed three major areas: (1) a theoretical study of the problem, including digital computer solutions of various facets; (2) the selection of components and assembly of a prototype deep ocean instrument; and (3) the development of calibration techniques for such an instrument. This has been a laboratory study using soil "models" rather than ocean sediments. It was felt that more basic information could be obtained from simple soils than from complicated ocean samples. Any ideas of using or adapting a commercial nuclear meter were quickly discarded, for no available meter was designed for depths greater than 200 feet. In addition, all used large detectors which diminish the spatial resolution of the instrument. It was also felt that more basic knowledge of the theory and parameter-dependence of moisture meters could be obtained if a non-commercial prototype instrument were constructed. Such an instrument would allow variations in many parameters which

are fixed in a commercial instrument (detector type, source-detector spacing, etc.).

Considerable efforts have been expended over the past thirty years in the development of instruments which can determine soil density and/or moisture without recourse to time-consuming core samples. Through this research a wide variety of nuclear density and moisture meters has been developed (7, p. 3-5). These instruments rely on the predictability of gamma ray (γ) and neutron attenuation and scattering in materials to determine the density and/or moisture content of the soil. The instruments may be the surface variety, which rely wholly on backscattered radiation, or the subsurface type, which actually is lowered down a hole to measure variation of density with depth. The instruments may have their radioactive sources in the same assembly as the radiation detector, or they may have them in separate probes.

Development began in the early 1940's with Pontewino's development of a well-logging instrument using a neutron source and a ionization chamber. This was developed for use in petroleum exploration. In 1949, Pieper measured soil moisture content using a fast neutron source and an indium foil detector. The year 1950 ushered in a period of considerable research with subsurface meters. By 1952, a surface meter had been developed. During the mid-1950's, the foil detectors were replaced by proportional counters and other forms of direct

reading apparatus, and water and paraffin came into common use as calibrating media. The first subsurface moisture meter was sold in Australia in 1956; the first surface meter was sold in 1958 in New Zealand. Subsurface meters became readily available commercially in 1957 and surface meters in 1959. By 1960, artificial media were being used for calibration in place of actual soils.

Since 1960, most work has been done in refinement of the instruments, in improving calibration techniques, and in boundary layer studies. The standard commercial meters still employ proportional counters and use portable, direct reading ratemeters or strip chart recorders. Most of the moisture meters constructed to date have monitored a thermal (~0.025 eV) neutron flux. Unfortunately, the response of such instruments is greatly affected by the solids in the soil or sediment. Wilson and Youmann (8, p. 9-14) have suggested a device measuring epithermal neutron flux.

The aim of this project is to investigate such a device--an epithermal neutron moisture meter capable of in situ measurements leading to moisture content. The general theory of moisture measurement by neutron moderation is developed, different types of neutron sources and detectors are examined, and the associated electronic amplification and readout systems are chosen. Various soil models are mixed and their moisture content measured with the prototype instrument. The prototype instrument was constructed so that the

maximum number of parameters could be varied and investigated. A general discussion of the results of these measurements follows, and some conclusions are drawn. Design specifications for the final instrument are given; as are recommendations for further studies along these lines.

As it is realized that this paper may be read and/or utilized by persons of varying disciplines, an explanation of symbols used is included in Appendix I.

II. GENERAL NEUTRON MOISTURE INSTRUMENT THEORY

Operation of most nuclear moisture meters is based on the principle of measuring the number of neutrons emitted from a high energy source which reach a lower energy. In most cases, this lower energy is thermal energy; that is, that energy at which the neutron is in thermal equilibrium with its environment. Thermal energy is generally chosen as the interval of observation because neutrons of this energy are easiest to detect. To observe neutrons in another energy interval, a more sophisticated type of detector is required.

Each element possesses a finite probability for undergoing an interaction with a neutron. This is called the total neutron cross section and may be considered in the one atom, or microscopic sense (σ_T), or as the interaction probability of all atoms and/or elements present (Σ_T). The total cross sections Σ_T and σ_T are really sums of probabilities or cross sections for different atom-neutron interactions. The most important of these cross sections are those for scattering and absorption.

The nuclear moisture meter is based on the predictability of these neutron interactions in matter, and its operation is almost directly related to the macroscopic scattering cross section (Σ_s) of the hydrogen in water. The higher the water (hence hydrogen) content in a soil, the

higher the value of Σ_s. If Σ_s increases, the neutron scattering rate increases relative to the neutron absorption rate. More neutrons thus lose energy by scattering processes and are available in the medium at low energies. Hence the number of low energy neutrons can be related directly to the water content.

A neutron captured by an element in the medium under consideration obviously cannot be counted at the detector. This probability of elemental capture of a neutron is known as the macroscopic neutron absorption cross section (Σ_a); the probability of capture by one atom of an element is the microscopic absorption cross section (σ_a). The reaction itself is given by

$$ {}_zX^A + n \rightarrow {}_zX^{A+1} + \gamma $$

where X is the element of atomic number Z and atomic weight A. Σ_a of an element will vary with the energy of the incident neutrons, with the atomic or molecular concentration of the particular element (number density N), and to a much lesser extent with temperature. Σ_a can be described by

$$ \Sigma_a(E) = N\sigma_a(E) \qquad \text{(II-1)} $$

where E is the neutron energy and $\sigma_a(E)$ is proportional to $1/E$ for most of the significant constituents of a marine sediment. Elements with relatively high absorption cross sections found in ocean

sediments are boron, cadmium, chlorine, iron, manganese, and sodium. These elements have their highest value of absorption cross section at very low energies (e.g., thermal energy) and their cross section decreases at higher energy.

Due to the fact that its atomic weight is essentially the same as the neutron's, hydrogen is the most efficient elastic scatterer of neutrons. Not only does it possess a relatively high microscopic scattering cross section (σ_s) (20 barns for H, 103 barns for H_2O at thermal energies), but the average neutron energy loss per collision with H is equal to one-half the incident energy. This coupled with the fact that the maximum fractional energy loss per collision decreases with increasing mass of the struck nucleus makes hydrogen the best elastic scatterer known (3, p. 167-184).

Other light elements present in a sediment may also scatter neutrons; e.g., the carbon in a $CaCO_3$ sediment. However, as mentioned above, as atomic weight increases, the fractional neutron energy loss per collision decreases, and hence the number of collisions to slow down the neutron to a given energy increases. For instance, the slowing of neutrons from an average energy of 2 MeV to 1 eV requires 14.5 collisions in a hydrogen medium, 91.3 collisions in a carbon (graphite) medium, or 407 collisions in iron (3, p. 186). Hence unless a mixture contains an extraordinarily large concentration of some other light element, the effectiveness of the medium in slowing down

neutrons will be indicative of its hydrogen content. If most of the hydrogen present in a sediment is in the molecule H_2O, the sediment's effectiveness as a slowing down medium will be indicative of the amount of water present.

One other scattering mechanism, inelastic scattering, could also contribute to the number of low energy neutrons in a material. However, to undergo an inelastic collision, a neutron must be initially at a very high energy, e.g., 4.8 MeV in carbon or 6.4 MeV in oxygen. This type of scattering can be avoided by picking a source whose spectrum is concentrated about 1 to 2 MeV.

Thus when high energy neutrons are injected into a medium, the mechanisms of scattering and absorption are available. As long as the energy of the neutron is high (about 1 eV to 2 MeV) scattering generally predominates over absorption and the scattering ability of the medium is governed almost exclusively by the water present. When the neutron reaches thermal energies (0-1 eV), absorption becomes an important mechanism, and the amount of absorption is directly related to the composition of the medium through Σ_a. Thus a measurement of the number of thermal neutrons present is <u>not</u> directly related to the number of scattered neutrons and hence the water content; the absorption process has removed some of these neutrons and made the measurement dependent on the composition of the medium.

This problem can be eliminated by measuring the number of neutrons in an energy range where scattering is still predominant and absorption processes are small to negligible. Such an energy range is the epithermal range (1-10 eV). Neutrons measured in this range are essentially only scattered neutrons, their number is directly related to the water content, and the measurement is not dependent on the composition of the medium.

The movement of neutrons in a medium may be approximated with good accuracy by diffusion theory. As discussed in most reactor theory or neutron physics texts (4, p. 160-198), diffusion theory describes the motion of neutrons in any medium by

$$\frac{\partial n(\vec{r}, t, E)}{\partial t} = s(\vec{r}, t, E) - \Sigma_a(\vec{r}, E)\, \phi(\vec{r}, t, E) - \operatorname{div} \vec{J}(\vec{r}, t, E) \qquad \text{(II-2)}$$

where

$\vec{r}$ = the position vector

n = number of neutrons per unit volume

t = time

E = energy

s = strength of any neutron source in the medium

ϕ = the neutron flux (the total track length of all neutrons at a given energy per unit volume and time)

$\vec{J}$ = neutron current density vector (net number of neutrons

crossing a unit area per second normal to the area).

In most cases it can be shown that for a large, steady state, weakly absorbing, sourceless medium

$$\vec{J}(\vec{r}, E) = -D(\vec{r}, E) \text{ grad } \phi(\vec{r}, E) \qquad \text{(II-3)}$$

where $D(\vec{r}, E)$ is a proportionality constant called the diffusion coefficient.

$$D = \frac{\Sigma_s}{3\Sigma_t^2} \text{ from diffusion theory}$$

or (II-4)

$$D = \frac{1}{3\Sigma_s(1-\bar{\mu})}, \quad \bar{\mu} = \frac{2}{3A} \text{ from transport theory}$$

where

Σ_t = the total macroscopic interaction cross section

$\bar{\mu}$ = the average of the cosine of the neutron scattering angle

A = the atomic weight of the element or molecule under consideration.

Considering only monoenergetic neutrons, Eqn. (II-2) further reduces to

$$\text{div } [D(\vec{r}) \text{ grad } \phi(\vec{r})] - \Sigma_a(\vec{r})\phi(\vec{r}) + s(\vec{r}) = 0$$

If the medium is homogeneous, D and Σ_a are no longer functions of position and the final neutron diffusion equation results:

$$D\nabla^2\phi(\vec{r}) - \Sigma_a\phi(\vec{r}) + s(\vec{r}) = 0 \qquad \text{(II-5)}$$

In this monoenergetic case, neutron flux $\phi(\vec{r}) = nv$; where n is

the neutron density and v is the velocity of the neutrons.

Consider then a point source emitting S monoenergetic neutrons per second isotropically in an infinite medium. In spherical coordinates, Eqn. (II-5) is given by

$$\frac{1}{r^2}\frac{d}{dr}r^2\frac{d\phi}{dr} - \frac{1}{L^2}\phi = 0$$

where $L^2 = D/\Sigma_a$ and is known as the diffusion length. L is a measure of the distance a neutron travels between entry into a system and loss from the system. In this case it is the distance between the source and the point of absorption. Solutions to this diffusion equation are

$$\phi(r) = \frac{Ce^{-\frac{r}{L}}}{r} + \frac{Fe^{\frac{r}{L}}}{r} \qquad \text{(II-6)}$$

where C and F are constants to be determined. The contribution of the source is treated as a boundary condition; namely, that the net number of neutrons passing through a sphere of radius "r" about S must be given by $4\pi r^2 J(r)$.

Hence

$$\lim_{r\to 0} r^2 J(r) = \frac{S}{4\pi}$$

A second boundary condition is obvious, since S is finite,

$$\lim_{r\to\infty} \phi(r) = 0$$

Inserting these boundary conditions into Eqn. (II-6) one sees that

$$F = 0$$

$$J(r) = -D\frac{d\phi}{dr} = DC\left(\frac{1}{rL} + \frac{1}{r^2}\right) e^{-\frac{r}{L}}$$

$$\lim_{r \to 0} r^2 J(r) = \lim_{r \to 0} DC\left(\frac{r}{L} + 1\right) e^{-\frac{r}{L}} = \frac{S}{4\pi}$$

$$C = \frac{S}{4\pi D}$$

Hence the flux caused by a monoenergetic source in an infinite medium is

$$\phi(r) = \frac{Se^{-\frac{r}{L}}}{4\pi Dr} \qquad \text{(II-7)}$$

Going one step further, consider two concentric spheres of different material surrounding a point source of strength S. The inner sphere has radius R and diffusion length L_1, and the outer sphere has an infinite radius and diffusion length L_2. Then Eqn. (II-5) becomes

$$\frac{1}{r^2}\frac{d}{dr} r^2 \frac{d\phi}{dr} - \frac{1}{L_1^2}\phi = 0 \qquad 0^+ < r < R$$

and

$$\frac{1}{r^2}\frac{d}{dr} r^2 \frac{d\phi}{dr} - \frac{1}{L_1^2}\phi = 0 \qquad r > R$$

Boundary conditions are

(i) $\lim_{r \to 0} r^2 J(r) = \frac{S}{4\pi} \qquad 0^+ < r < R$

(ii) $\phi(R^-) = \phi(R^+)$

$$\text{(iii)} \qquad D_1 \frac{d\phi(R^-)}{dr} = D_2 \frac{d\phi(R^+)}{dr}$$

$$\text{(iv)} \qquad \lim_{r \to \infty} \phi(r) = 0 \qquad\qquad r > R$$

For solutions:

$$\phi(r) = \frac{C_1 \sinh \frac{r}{L_1}}{r} + \frac{F_1 \cosh \frac{r}{L_1}}{r} \qquad 0^+ < r < R$$

$$\phi(r) = \frac{C_2 e^{-\frac{(r-R)}{L_2}}}{r} + \frac{F_2 e^{-\frac{(r-R)}{L_2}}}{r} \qquad r > R$$

Applying

$$\text{(i)} \qquad \text{gives} \quad F_1 = \frac{S}{4\pi D_1}$$

$$\text{(iv)} \qquad \text{gives} \quad F_2 = 0$$

and (ii) and (iii) gives

$$C_1 = \frac{S}{4\pi D_1} \frac{L_1(D_2R + D_2L_2 - D_1L_2)\cosh \frac{R}{L_1} + D_1L_2R \sinh \frac{R}{L_1}}{L_1(D_1L_2 - D_2R - D_2L_2)\sinh \frac{R}{L_1} - D_1L_2R \cosh \frac{R}{L_1}}$$

$$C_2 = C_1 \sinh \frac{R}{L_1} + \frac{S}{4\pi D_1} \cosh \frac{R}{L_1}$$

Hence

$$\phi(r) = \frac{C_1 \sinh \frac{r}{L_1}}{r} + \frac{S}{4\pi D_1 r} \cosh \frac{r}{L_1} \qquad 0^+ < r < R$$

$$\phi(r) = \frac{C_2 e^{-\frac{(r-R)}{L_2}}}{r} \qquad r > R \qquad \text{(II-8)}$$

As can be seen from the above, the analytic solution for the simple geometry of two concentric spheres becomes quite complicated. Additionally, the derivations above are for monoenergetic neutrons; to properly model any moisture measuring instrument, energy dependence must be included. This gives a diffusion equation of the form

$$-D(E)\nabla^2\phi(\vec{r}, E) + \Sigma_a(E)\phi(\vec{r}, E) - s(\vec{r}, E) = 0 \qquad \text{(II-9)}$$

where $D(E)$ and $\Sigma_a(E)$ are constant within a spatial region. If $D(E)$, $\Sigma_a(E)$ and $s(\vec{r}, E)$ are very simple, well-behaved functions, Eqn. (II-9) can be solved exactly. Since this is the exception rather than the rule, numerical methods are normally used to solve for $\phi(\vec{r}, E)$.

Most numerical schemes divide the energy range of interest into intervals and then find average values of D, Σ_a, and S over each interval. These parameters then become energy independent within the interval, Eqn. (II-9) becomes dependent only on position, and a monoenergetic "group" flux is obtained. Hence these schemes are called multigroup schemes.

A typical group equation in a non-multiplying (non-fission) medium in which only scattering to lower energies is allowed would be

$$D_g \nabla^2 \phi_g(\vec{r}) - \Sigma_{ag}\phi_g(\vec{r}) - \sum_{h>g}^{G} \Sigma_s(g\rightarrow h)\phi_g(\vec{r}) + \sum_{h=1}^{g-1} \Sigma_s(h\rightarrow g)\phi_h(\vec{r}) + S_g(\vec{r}) = 0 \qquad \text{(II-10)}$$

where G = number of groups, and

$$\phi_g(\vec{r}) = \int_{E_{g-1}}^{E_g} \frac{\phi(\vec{r}, E)dE}{E}$$

Letting

$$\phi'_g = \int_{\Delta E} \frac{\phi(E)dE}{E}$$

$$D_g = \frac{\int_{E_{g-1}}^{E_g} \frac{D(E)\phi(\vec{r}, E)dE}{E}}{\int_{E_{g-1}}^{E_g} \frac{\phi(\vec{r}, E)dE}{E}} = \frac{1}{\phi'_g} \int_{\Delta E} \frac{D(E)\phi(E)dE}{E}$$

since it is assumed that flux is a separate function of space and energy.

The group cross section are given by

$$\Sigma_{ag} = \frac{1}{\phi'_g} \int_{\Delta E} \frac{\Sigma_a(E)\phi(E)dE}{E}$$

$$\Sigma_s(i\rightarrow j) = \frac{1}{\phi'_i} \int_{\Delta E}\int_{\Delta E'} \frac{\Sigma_s(E)P(E\rightarrow E')dEdE'}{EE'}$$

where $P(E \rightarrow E')$ is the probability of scattering from interval dE about E into interval dE' about E'. Often a new function

$$\Sigma_{rg} = \Sigma_{ag} + \sum_{h>g}^{G} \Sigma_s(g \rightarrow h) \qquad \text{(II-11)}$$

is used for simplicity. Σ_{rg} is called the removal cross section for group g.

The group source term is given by

$$S_g(r) = \int_{\Delta E} \frac{s(r,E)dE}{E}$$

Although Eqn. (II-10) appears quite complicated, it is readily solved by a computer. Normally one computer program will be used to generate the various group constants. Once these are obtained, another computer program solves the diffusion equation.

A one-dimensional solution of Eqn. (II-10) in a non-multiplying medium is quite simple and very fast. Using the approximation,

$$\left.\frac{\partial \phi}{\partial r}\right|_{r_{k+\frac{1}{2}}} = \frac{\phi_{k+1} - \phi_k}{r_{k+1} - r_k}$$

a tridiagonal matrix results for each energy, the order of the matrix depending on the number of space points. This system of equations can be solved without iteration. The flux in the highest energy group is found first. Then using this information, Eqn. (II-10) is solved for the next lower group. This continues until all group fluxes are

specified. Unfortunately solutions for more than one dimension require iteration and hence the codes run more slowly and require much more memory storage in the computer.

The analytical solutions for the project were obtained using a Battelle Northwest code, HFN, and a code written especially for the project, SEAN. HFN is a massive reactor diffusion theory code which will also solve fixed source problems such as this. However, it requires considerable computer memory as well as having many more reactor options than are necessary. Hence SEAN was written. Certain of its results have been checked against HFN to be sure they agree, as well as checking against the exact solution of a point source in a infinite medium. A listing of SEAN will be found in Appendix II.

Both SEAN and HFN were run for ten (10) energy groups. This number was chosen as giving a good representation of energy variation without using an inordinate number of energy groups. The literature indicated that the Am-Be source spectrum was very similar to a Po-Be source spectrum. Hence a 1/E flux distribution from a Po-Be source was the input to another Battelle code, HRG. From this, group constants for groups 1 through 9 were determined. Battelle's THERMOS code was used to generate the thermal (group 10) constants. The 1/E flux was used because it is a good approximation to what actually occurs in a weakly absorbing medium. The group divisions are shown in Table 1.

Table 1. Group Structure for Multigroup Solutions.

Group	Energy Range (eV)
1	$> 2.23 \times 10^{6}$
2	$4.98 \times 10^{5} - 2.23 \times 10^{6}$
3	$1.11 \times 10^{5} - 4.98 \times 10^{5}$
4	$2.48 \times 10^{4} - 1.11 \times 10^{5}$
5	$5.53 \times 10^{3} - 2.48 \times 10^{4}$
6	$1.23 \times 10^{3} - 5.53 \times 10^{3}$
7	101 - 1230
8	10.68 - 101
9	0.414 - 10.68
10	< 0.414

Group 9 is referred to as the Epithermal Group

Group 10 is referred to as the Thermal Group

As discussed above, the low energy flux from a neutron source in a non-multiplying medium is indicative of the hydrogen and hence the water concentration. The thermal neutron flux is by far the easiest to measure and is also the greatest in magnitude. This is the flux in the energy interval below 1 eV and centered about 0.025 eV. Most neutron moisture meters use this flux as the basis of their measurements. A precise measurement of the water content can be obtained if the instrument is calibrated for the particular soil type.

The thermal flux is greatly affected by absorption of neutrons by the constituents of the sediment as well as by the water contained therein. For thermal energies, elements such as boron (σ_a = 759 b), chlorine (σ_a = 33 b), manganese (σ_a = 13.3 b) and many others have absorption cross sections of the same order of magnitude as the scattering cross section of water (σ_s = 103 b), and hence they can greatly effect the thermal flux. Thus any calibration of a thermal neutron meter presupposes a knowledge of the constituents of the soil. Figures 1 and 2 show the effect of boron and chlorine concentrations on the flux in water.

Interestingly enough, neutron measurements at this energy can be somewhat more indicative of water content than higher energy measurements. Below about 1 eV, the neutron no longer sees two free hydrogen and one free oxygen atom. Instead, the molecule H_2O becomes the target nucleus and σ_s increases from about 20 b at

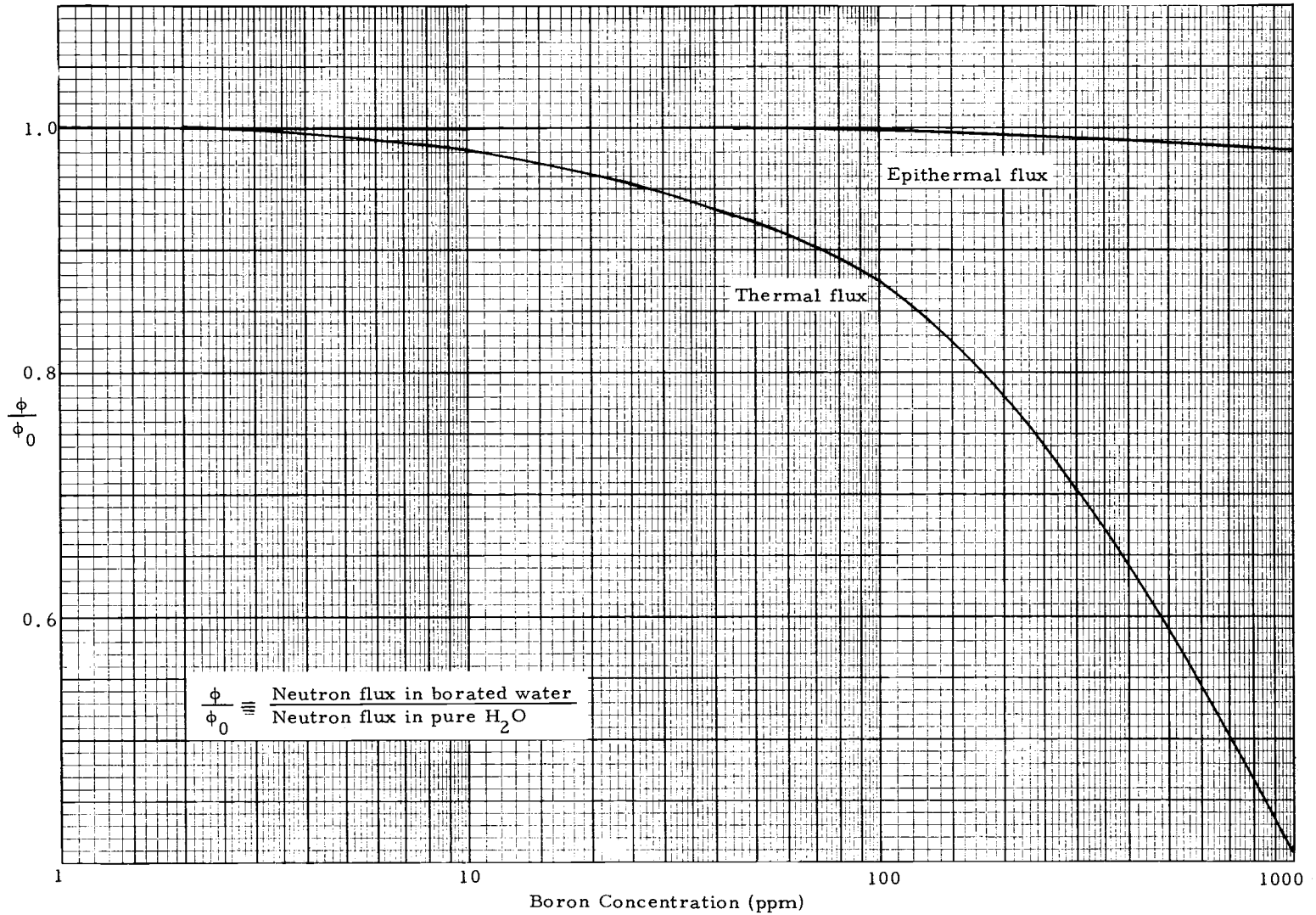

Figure 1. Variation in Thermal and Epithermal Neutron Flux in Water with Variation in Boron Concentration (curves generated by SEAN).

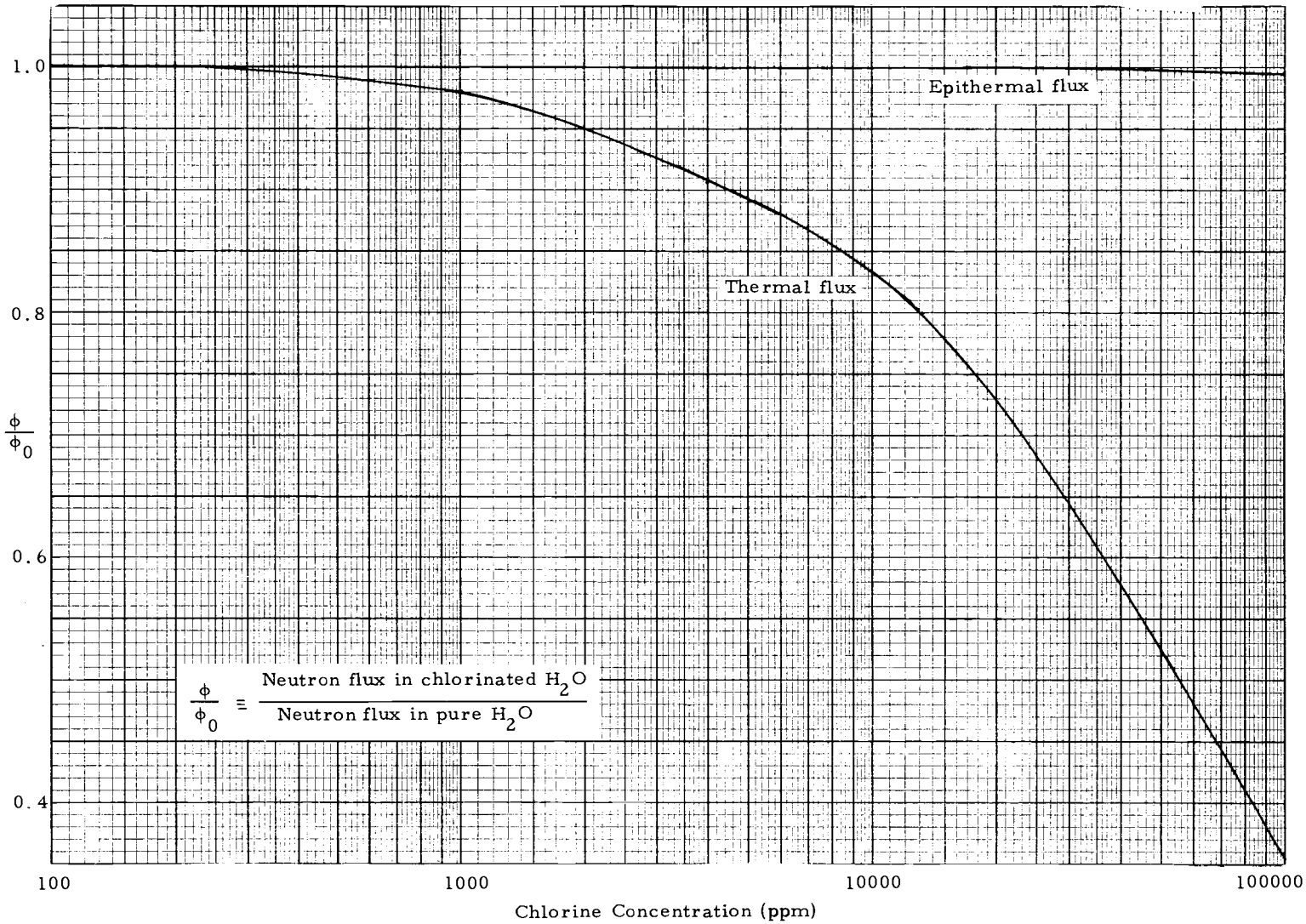

Figure 2. Variation of Thermal and Epithermal Neutron Flux in Water with Variation in Chlorine Concentration (curves generated by SEAN).

1 eV to 103 b at 0.025 eV. This minimizes the effects of any hydrogen bound in any other molecules. Still, however, there is no way to absolutely distinguish between the hydrogen in soil structure or in bound water and the hydrogen in free water.

As discussed in Section IV, it is relatively simple to construct a detector to count neutrons of energies from 1 to 10 eV. These are the epithermal neutrons. Measurements in this range are rather insensitive to the composition of the sediment since the σ_a's of the high absorbers have substantially diminished due to their $1/\sqrt{E}$ dependence. The value of σ_s of water has dropped only from about 100 to 40 b. Hence, it is conceivable that an instrument operating in this energy range could measure water content without prior knowledge of the sediment. Curves of the effects of boron and chlorine concentration on epithermal flux are also shown in Figures 1 and 2.

Measurement of epithermal flux has one other advantage. The epithermal energy is greater than the binding energy of molecules; hence, the atoms of a molecule are "seen" individually by a neutron. Thus, in predicting the flux, the molecular cross sections are not needed; instead the parameters for the individual elements in the mixture can be used.

Unfortunately, epithermal flux is about a factor of ten lower in magnitude than the thermal flux. This is due to the large number of neutrons scattered into the thermal group. Use of a large source or

longer counting times will normally ensure an adequate number of counts and eliminate this problem.

It is readily seen from the homogeneous neutron diffusion equation that the diffusion length

$$L = \sqrt{\frac{D}{\Sigma_a}}$$

is a measure of the "attenuation" length of the space-dependent flux, roughly analogous to the time constant in time-variant systems. For the simple case of the point source in the infinite medium, L is the relaxation length; i.e., in distance L the flux falls off by a factor of e.

Since

$$L = \sqrt{\frac{D}{\Sigma_a}}$$

and D and Σ_a are determined by the type of material, L must also be dependent on material. Typical values for L in various materials at thermal energies and 20°C are (1, p. 113, 109, 107)

Material	L (cm)
H_2O	2.8
Be	21
Graphite	54

Since constants for mixtures are normally weighted averages of the constants of the constituents, it is readily apparent that L for a sediment mixture will vary with the concentration of components of

the mixture including the water.

Along with being dependent on material composition, L is also dependent on neutron energy. Simply put, this means that the average distance traveled before removal (L) is a function of the energy of the neutron. But since D(E) and $\Sigma_a(E)$ vary with energy and material in an independent and unrelated manner, it is difficult to make a general statement of the variation in L with energy.

As discussed above, the low energy neutron flux in a water-sediment mixture is directly related to the number of water molecules present. In the epithermal energy group, the flux appears to be proportional to the water content. Since these scattering and absorption relations are expressions for neutron-atom or neutron-molecule collisions or absorptions, it is the number of water molecules (or hydrogen atoms, boron atoms, etc.) per unit volume which is important in analyzing and calibrating a moisture detection instrument. The macroscopic probability or cross section of reaction is the product of the cross section per atom and the number of atoms per unit volume:

$$\Sigma = N\sigma$$

This number density is defined as

$$N = \left(\frac{m}{V}\right)\left(\frac{N_0}{A}\right) \qquad \text{(II-12)}$$

where

m is the mass of the material present in volume V (This definition becomes very important in mixtures.)

N_0 is Avogadro's number

A is the atomic weight of the atom (or molecular weight of a molecule) whose N is being calculated.

It is often convenient to define atom percent. This is

$$\text{Atom Percent of } i^{th} \text{ Type of Atoms} = \frac{(\text{number of atoms or molecules of one kind per unit volume})(100)}{\text{total number of atoms or molecules per unit volume}}$$

or

$$(a/o)_i = \frac{N_i}{N} \qquad \text{(II-13)}$$

where

N_i is number density of i^{th} type of atoms or molecules

N is the total number density of all types of atoms or molecules

In this study the atom percent of water is the most important quantity of this type; hence it is designated simply as (a/o). Unfortunately, most civil engineers measure water content in terms of moisture w. Hence, the relation is developed to relate w and a/o.

$$\frac{w}{100} = \frac{m_{H_2O}}{m_{solid}}$$

$$a/o = \frac{100\, N_{H_2O}}{N_{H_2O} + N_{solid}}$$

and

$$N_{H_2O} = \frac{m_{H_2O}}{V_{total}} \quad \frac{N_0}{A_{H_2O}}$$

$$a/o = \frac{\dfrac{m_{H_2O}}{18}\,(100)}{m_{solid}\left[\dfrac{m_{H_2O}}{18 m_{solid}} + \dfrac{1}{A_{solid}}\right]},$$

since $A_{H_2O} = 18$. Thus

$$a/o = \frac{\dfrac{100w}{1800}}{\dfrac{w}{1800} + \dfrac{1}{A_{solid}}}$$

$$a/o = \frac{100w\, A_{solid}}{wA_{solid} + 1800}$$

or

$$w = \frac{1800\, a/o}{A_{solid}(100 - a/o)} \qquad \text{(II-14)}$$

One can also relate a/o and w for materials not having definite atomic weight, e.g., clays, mixtures, etc., by the following:

$$\rho = \frac{N_{solid} A_{solid}}{N_0} + \frac{N_{H_2O} A_{H_2O}}{N_0} \qquad \text{(II-15)}$$

where ρ is the mass density of the soil. But

$$a/o = \frac{100\, N_{H_2O}}{N_{H_2O} + N_{solid}} \qquad \text{(II-16)}$$

Rearranging Eqn. (II-16) gives

$$N_{solid} = \frac{N_{H_2O} (100 - a/o)}{a/o} \qquad \text{(II-17)}$$

Now

$$N_{H_2O} = \frac{V_{H_2O} N^0_{H_2O}}{V_{total}} \qquad \text{(II-18)}$$

where

$N^0_{H_2O}$ = the number density of pure water

V_{H_2O} = the volume occupied by water in the mixture

V_{total} = the total volume of the mixture.

Then

$$\frac{V_{H_2O}}{V_{total}} = \frac{N_{H_2O} V^0_{H_2O}}{N_{H_2O} V^0_{H_2O} + N_{solid} V^0_{solid}} \qquad \text{(II-19)}$$

where

$V^0_{H_2O}$ = the volume occupied by one water molecule

V^0_{solid} = the volume occupied by one molecule of solid.

If one assumes

$$V^0_{H_2O} = V^0_{solid} \tag{II-20}$$

then from Eqn. (II-19):

$$\frac{V_{H_2O}}{V_{total}} = \frac{N_{H_2O}}{N_{H_2O} + N_{solid}} = \frac{a/o}{100} \tag{II-21}$$

Substituting Eqn. (II-21) into Eqn. (II-18):

$$N_{H_2O} = \frac{a/o\ N^0_{H_2O}}{100} \tag{II-22}$$

From Eqn. (II-14):

$$A_{solid} = \frac{1800\ a/o}{w(100 - a/o)} \tag{II-23}$$

Substituting Eqns. (II-17) and (II-23) into Eqn. (II-15) gives

$$\rho = \frac{N_{H_2O}}{N_0}\ (\frac{1800}{w} + 18) \tag{II-24}$$

since $A_{H_2O} = 18$.

Substituting Eqn. (II-22) into Eqn. (II-24) gives

$$\rho = \frac{a/_o \, N^0_{H_2O}}{100 \, N_0} \left(\frac{1800}{w} + 18\right) \qquad \text{(II-25)}$$

But for pure water

$$N^0_{H_2O} = \frac{\rho_{H_2O} \, N_0}{A_{H_2O}} = \frac{(1)N_0}{18} = \frac{N_0}{18} \qquad \text{(II-26)}$$

Substituting Eqn. (II-26) into Eqn. (II-25) yields

$$\rho = \frac{a/_o}{1800} \left(\frac{1800}{w} + 18\right) = a/_o \left(\frac{1}{w} + .01\right) \qquad \text{(II-27)}$$

Rearranging Eqn. (II-27):

$$w = \frac{a/_o}{\rho - 0.01 \, a/_o} \qquad \text{(II-28)}$$

Eqn. (II-28) says that if the density and atom percent water of a soil or sediment are known, the moisture content is specified. If then $a/_o$ and ρ can be measured accurately <u>in situ</u>, w can be determined without a sediment sample. The accuracy of this determination depends on the validity of the assumption in Eqn. (II-20).

The above considerations led to the decision to build a prototype subsurface nuclear meter which would measure the epithermal flux from a nearby source. A subsurface probe was selected for two reasons:

(1) A subsurface meter allows movement of the source/detector along the vertical; hence giving information to

greater sediment depths.

(2) Since the diffusion length for neutrons of any energy in high moisture sediments is on the order of 10 cm, the volume of sediment measured by the probe extends at best less than 10 inches from the source. This makes a surface meter rather useless for measuring moisture content to any reasonable depth.

The probe will be designed to measure primarily epithermal neutrons since these measurements should result in a water content which is sediment independent, or very nearly so.

The probe will be calibrated in a homogeneous mixture of solids and sea water. To approximate an infinite medium, there will be at least eight to ten inches of this soil on all sides; thus, neither equipment or material parameters will be affected by neutron leakage from the sample. Data will not be taken if there are extreme temperature variations.

III. NEUTRON SOURCES

There are many considerations in choosing a neutron source for a nuclear moisture meter. To limit radiological hazards, the strength must be minimized and the radioisotopes chosen to provide minimal danger to the operator. In order to predict the response of the instrument and to provide the utmost spatial resolution, the source should approach a point source. This in turn implies that the source has a reasonably high specific activity. Further, although its strength should not be a radiological hazard, the source must still produce enough neutrons to provide an adequate count rate. To fully understand the mechanisms involved in instrument operation, some knowledge of the source energy spectrum must be available. The source must also be available and reasonably priced. Finally, it should have a long enough half-life to be stable over the period of measurements.

Many types of neutron sources exist. Some such as Cf^{252}, a spontaneous fission source, must be ruled out at present due to their high cost and restricted availability. Source tubes and liquid or gaseous sources are too difficult to handle and too fragile for a deep ocean probe. Usable sources are of two types: photoneutron (γ, n) sources, and alpha-induced (α, n) sources. The (γ, n) sources can be eliminated due to the high energy γ's which they all emit. These

gamma rays will interact with the detector and make it very difficult to obtain a true neutron count rate. They also greatly increase the radiological hazards associated with the source.

Hence, the (α, n) source was chosen. Of the sources of this type, the most commercially available are Pu-Be, Po-Be, and Am-Be. The Po-Be source has the highest specific activity and hence the shortest half-life (138.4 days). It also emits a 0.8 Mev γ. The Am-Be source has a half-life of 458 years and a 0.06 Mev γ. The Pu^{239}-Be source has the longest half-life (24, 360 years) and the lowest γ yield; however, it is the greatest health hazard and requires a special licensing agreement with the Atomic Energy Commission since Pu^{239} is special nuclear material.

Using a (α, n) source has a great radiological advantage over a (γ, n) source; namely, that one need not shield against high energy γ's. The α's emitted are contained within the metal (usually stainless steel) capsule around the reactants. Hence, shielding is primarily against neutrons. Due to the double containers welded around the source materials, danger of surface contamination of the source is practically negligible if handled with reasonable care. Source strength varies with the source, but any which would be considered for a moisture meter could be adequately shielded rather easily. These sources are also small enough to allow application of the point source approximation.

After consideration of the above, an Am^{241}-Be source was chosen. An 89 mCi source was obtained, and this proved to be quite satisfactory. Its strength is 2.43×10^5 n/sec giving a dose rate at the surface of its holder of about 500 mrem/hour. Its eight inch diameter storage container filled with paraffin reduces the dose rate to 5 mrem/hour at the surface of the container. The Am-Be source was chosen because it exhibits a good specific activity with a reasonable half-life, and the effect of its 60 Kev γ is easily eliminated electronically by discrimination.

IV. DETECTORS AND ASSOCIATED EQUIPMENT

In designing a neutron detector assembly for deep ocean applications certain criteria must be satisfied. These are:

(1) For use to depths of 6,000 feet, the probe must be able to withstand pressures on the order of 3,000 psi.

(2) The probe must be operable in sea water.

(3) As many of the components as possible should be located out of the water.

(4) Signal transmission from the ocean floor to the ship should be good.

(5) Counting times should be as short as possible..

(6) The assembly should be relatively insensitive to changes in temperature. Pressure should be no problem as long as the assembly and cables are properly designed and sealed.

(7) Components should be interchangeable and easily replaced if necessary.

(8) The assembly should be as versatile as possible.

(9) The assembly should perturb the natural environment to the smallest degree possible.

Since the type of detector used with the assembly must meet the above criteria, certain things are specified for it. It must be highly sensitive to neutrons, while having as low a gamma sensitivity

as possible. The smaller it is, the easier it is to seal and the closer it is to being a point detector for comparison with analytical results. Detector efficiency should be as high as possible without increasing its size or sacrificing ruggedness or compactness. A low voltage detector is always preferred to minimize hazards to personnel and equipment and to hold down insulation and connection costs. Radiological problems associated with the detector should be virtually nonexistent or, at worst, minimal. Finally, the detector should be usable for either thermal or epithermal flux measurements.

The number of possible detectors is too large to consider a detailed discussion of all types. They may, however, be categorized into three basic types: gas chambers, scintillators, and semiconductor detectors. Price (6, p. 311-362) discusses all these, giving their advantages and disadvantages.

Gas chambers, such as BF_3 proportional counters, have the advantage of low γ sensitivity, ruggedness, and low cost. However, they have a low efficiency compared to other detectors and hence require a larger detector for a given count rate. Fission chambers utilizing U^{235} in a gas-filled tube can add to radiological problems since the detector as well as the source is then radioactive and must be licensed. Fission chambers are also more expensive and less rugged than BF_3 detectors.

Semiconductor devices are generally stable, low voltage

devices, either using a neutron absorber doped into the device or using the absorber as a radiator attached to the semiconductor. Both types are relatively expensive and neither is very rugged. These devices also have a low efficiency. The silicon surface barrier, a commonly used type, is principally a fast neutron detector, making it unsatisfactory for this application.

The literature seems to indicate that certain types of scintillation detectors give a high count rate with a small detector volume. Of these, a $Li^6I(Eu)$ detector has an efficiency of 90% or greater, and it would seem to be the best of the solid scintillation detectors. Properly encased, it is rugged. As with all detectors using photomultiplier tubes, it will operate in the 800-900 volt range. The liquid scintillators are ruled out because of their low density and hence low efficiency. Containment would be more of a problem with the liquid scintillators, and designing a rugged probe would be more of a challenge.

All the above detectors can be used for detecting epithermal as well as thermal neutrons by covering the detector with cadmium. This is more successful with the detectors using (n, α) reactions because the high energy of the α allows discrimination against the cadmium capture γ's.

The ideal container for detector and source will be made of a high-strength, corrosion-resistant metal with a low total neutron

cross section. Typical materials which fulfill two or more of these requirements are stainless steel, aluminum, copper-nickel, monel, and zircaloy. Theory indicates that zircaloy should be the best of these due to its negligible capture cross section, and it is as good as or superior to the other named materials with regard to strength and corrosion resistance.

The basic purpose of the detector assembly is to count thermal and/or epithermal neutrons emitted from a small source. Hence, there is no justification for any elaborate counting instruments. A preamplifier, linear amplifier, discriminator, and scaler-timer are all that are necessary. A single channel analyzer could also be used. Most commercial moisture meters use rate meters in their equipment. A rate meter, however, is not as accurate as a scaler-timer for determining count rates.

In order to reproduce data properly, a precise high voltage supply and a pulse generator are necessary. Also, a nuclear instrumentation module (NIM) bin is preferred for containing various components. This ensures that all sections of the system are operating at the same voltages as well as eliminating any need for batteries. The NIM bin is also well suited to shipboard use.

After consideration of the various aspects discussed above, it was decided to take data using the following equipment:

(1) A BF_3 detector to obtain responses of gas chamber detectors.

(2) A $Li^6I(Eu)$ detector with its voltage divider mounted integrally in the detector casing.

(3) A Gadolinium-loaded plastic scintillator with integrally mounted voltage divider. This was tested to attempt to find an efficient scintillator which was cheaper and more rugged than Li^6I.

(4) NIM Bin mounted counting equipment.

(5) Stainless steel, aluminum, and zircaloy-2 pipes to be tested as container materials.

V. EXPERIMENTAL MEASUREMENTS

Using the criteria discussed above, equipment was chosen to be tested for the prototype instrument. This is listed in Table 2. As more and more information was gathered, the aluminum and stainless steel pipes were found to be less satisfactory than the zircaloy-2 pipe, and they were no longer used. Toward the end of data taking, it was clear that the LiI detector was superior, and subsequent data were taken only with it.

Since a "typical" marine sediment is difficult to define, it was decided not to test simulated marine sediments but to test relatively pure samples of the constituents of most marine sediments. The range of marine sediments was considered to be represented by sand, "Red Clay", calcareous ooze, and siliceous ooze. Therefore, the materials for testing were selected to represent the composition of these sediments; these materials were calcium carbonate in the form of ground limestone, opal in the form of diatomaceous earth, silica sand (Ottawa density sand), and illite and montmorillonite clays. In all cases but one, these materials were used individually with sea water to form the test specimen. One sample containing a mixture of calcium carbonate, opal, and montmorillonite was tested. The basic material composition and the concentration of certain elements important in neutron interactions were determined through

Table 2. Equipment

Source

Monsanto No. MRC-N-SS-W AmBe-838

89 mcAm^{241}Be neutron of strength 2.43×10^{5} n/sec

Dimensions: Stainless Steel, 1/2" O.D. x 1/2" O.L.

Detectors

(1) N. Wood Counter Laboratory Model 6-10-5 BF_3 Proportional Counter (in brass).

(2) Harshaw Type 252/1.5-X, 1/2" diameter x 1/2" thick europium activated enriched lithium iodide crystal with coupled RCA 6199 phototube, all hemetically sealed in an aluminum container.

(3) Pilot gadolinium loaded (1/2% by weight) plastic scintillator, 1" diameter x 1" thick. Locally mounted on RCA 6199 phototube.

Piping

(1) 39" long, 2-7/8" O.D. x 3/8" wall, zircaloy-2 pipe.

(2) 48" long, 2" I.D. x 0.218" wall, schedule 80 aluminum pipe.

(3) 36" long, 3" O.D. x 2" I.D., T316 stainless steel tubing (0.400" wall thickness).

Counting Equipment (All Canberra Industries)

(1) Model 800 NIM Bin and Low Voltage Power Supply

(2) Model 805 Scintillation Detector Preamplifier

(3) Model 806 Proportional Counter Preamplifier (3KV Operation)

(4) Model 816 Spectroscopy Amplifier

(5) Model 895 Nuclear Counter (Option 01)

(6) Model 1407 Reference Pulser

(7) Model 3002 High Voltage Power Supply

chemical and neutron activation analysis. The results of these determinations are shown as Table 3.

Various parameters of the moisture meter were examined, usually involving the single probe moisture meter. A typical instrument setup is shown in Figures 3 to 6. The experiments performed are outlined below.

1. Output energy spectrums for the LiI and Gd detectors. The output of each detector was observed on a 400 channel analyzer to ensure that the high voltage, amplifier gain, and discriminator setting was proper for the particular detector. This was necessary to ensure that neutrons and not gammas were being counted. See Figures 7 and 8. The first indication that the gadolinium-loaded detector might not work well as an epithermal detector was observed here, for its spectrum with and without a cadmium cover was virtually the same. This is demonstrated by the close proximity of the curves in Figure 8.
2. Variation in count rate for the LiI detector as source-detector distance is varied. Curves of this information are shown in Figures 9 and 10 for various mixtures. The shape of these curves suggested the use of a five inch source-detector (S-D) distance for epithermal counting, a one inch (S-D) distance for thermal counting, and a five inch (S-D)

Table 3. Analysis of Soil Constituents.

Constituent	Basic Composition	Boron (ppm)	Chlorine (ppm)	Iron (ppm)
Sea water	100% H_2O	2.84	22,778	400
Limestone	98.2% $CaCO_3$	141.3	79.1	26,040
Sand	99% SiO_2		15.2	18.5
Opal	92% SiO_2, 4% Al_2O_3	455.1	1,039	6,880
Montmorillonite	58% SiO_2, 23% Al_2O_3	222.2	3,340	42,600
Illite	~60% SiO_2, ~30% Al_2O_3	150.9	849	57,200

Constituent	Manganese (ppm)	Sodium (ppm)	Density (gm/cm^3)
Sea Water		11,504	1.00
Limestone	108.9	80.3	2.72
Sand	54	25.8	2.67
Opal	203	3,075	2.16
Montmorillonite	159	10,900	2.86
Illite	2,505	617	2.755

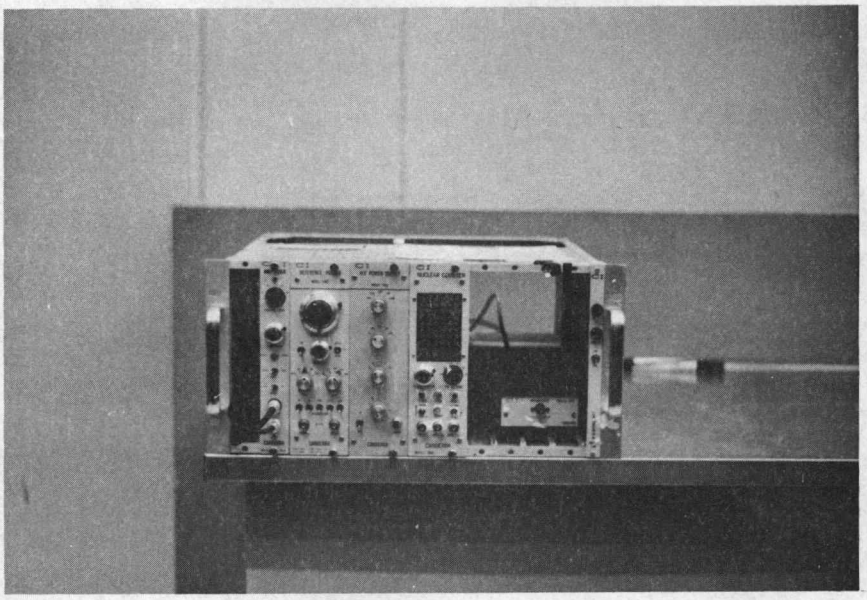

Figure 3. Front View of Moisture Meter Neutron Counting Equipment.

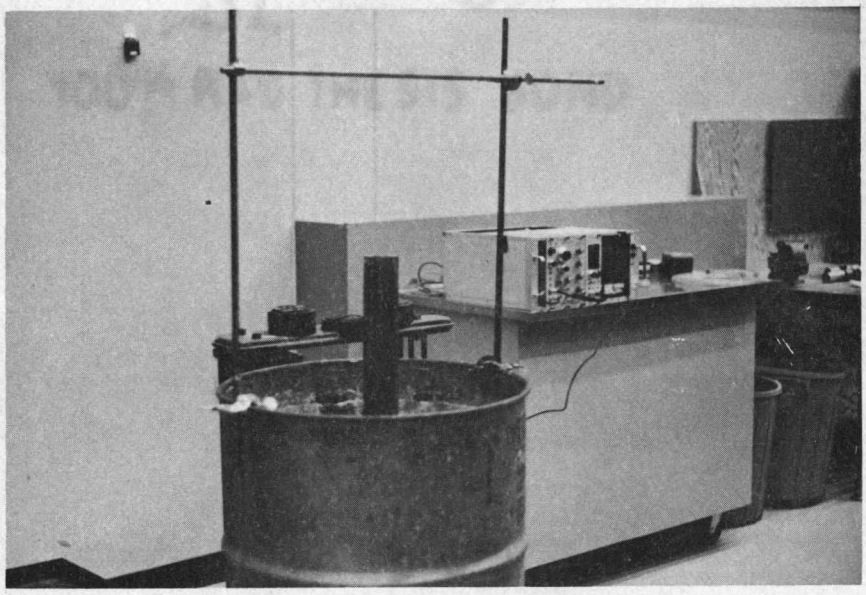

Figure 4. Side View of Moisture Test Stand (Counting Equipment in Background).

Figure 5a. Top View of Test Stand (Detector in Soil).

Figure 5b. Top View of Detector Entering Zircaloy Pipe.

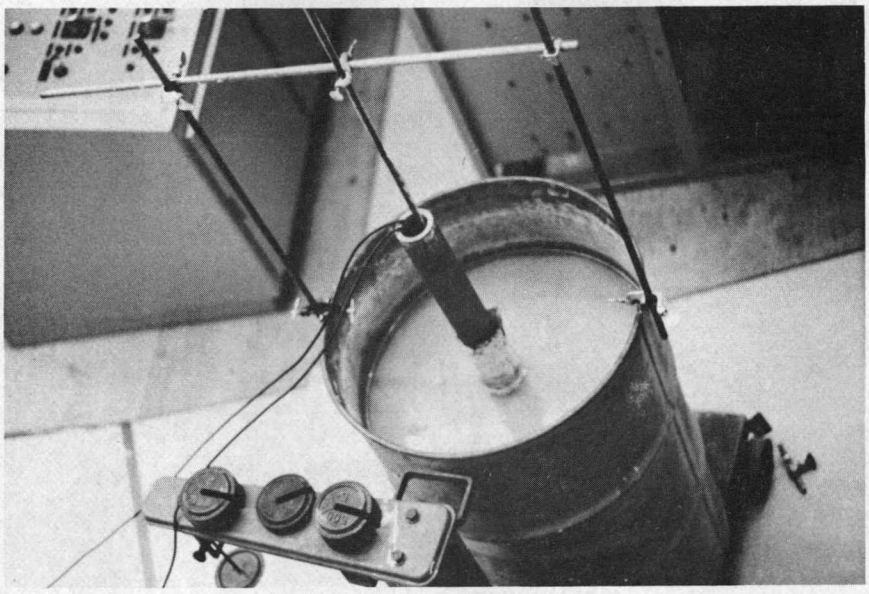

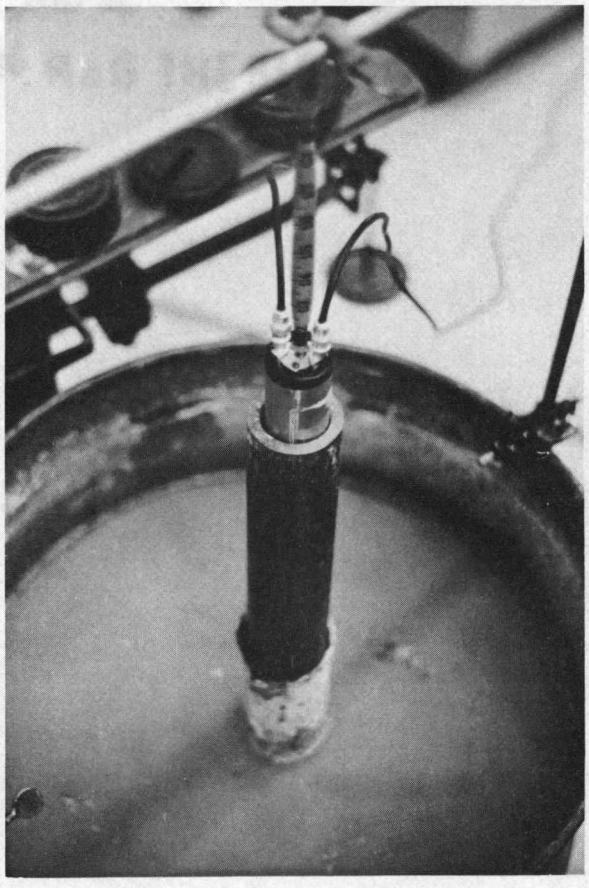

Figure 6a. Side View of Detectors and Source Holder. Top to Bottom: BF_3 Detector, $Li^6I(Eu)$ Detector, Gd Detector.

Figure 6b. End View of Detectors and Source Holder, Detector End Plate Not Attached. Left to Right: BF_3 Detector, $Li^6I(Eu)$ Detector, Gd Detector.

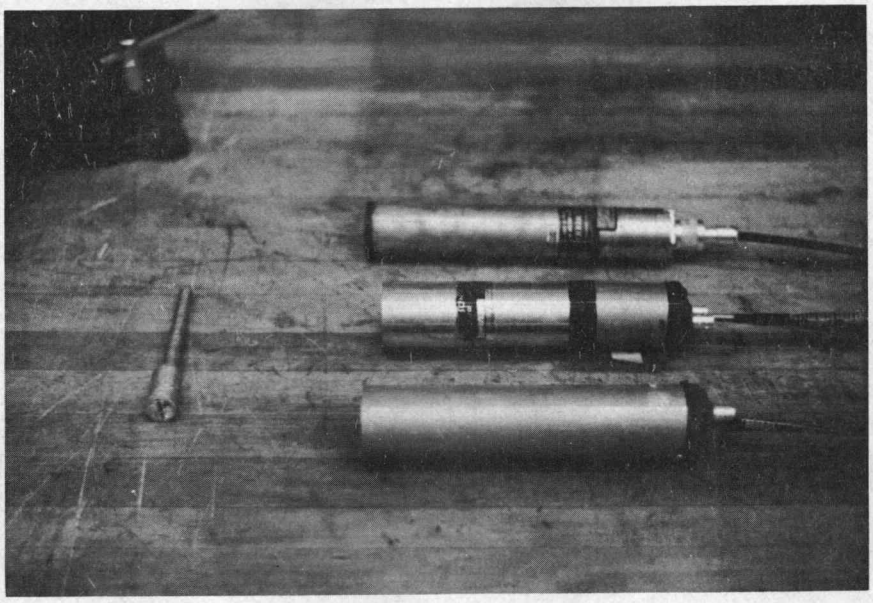

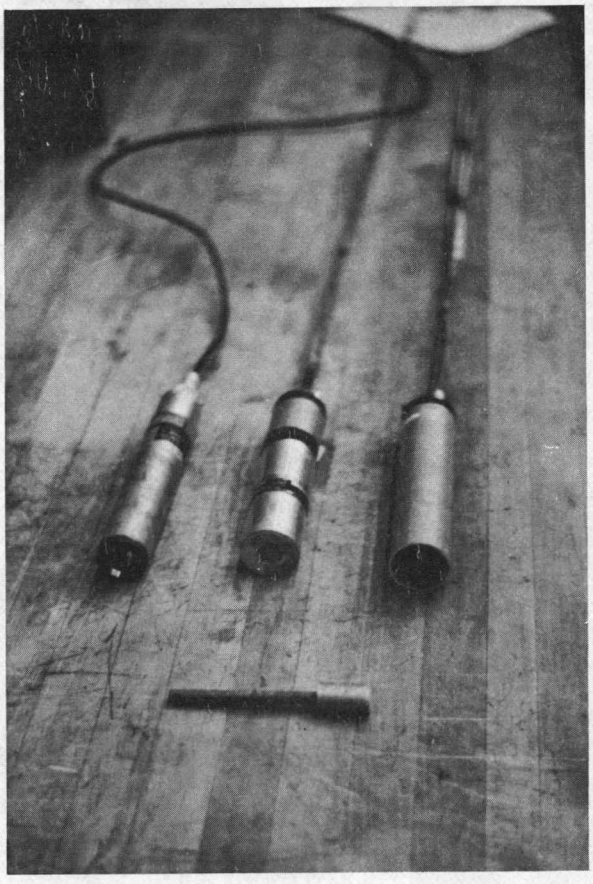

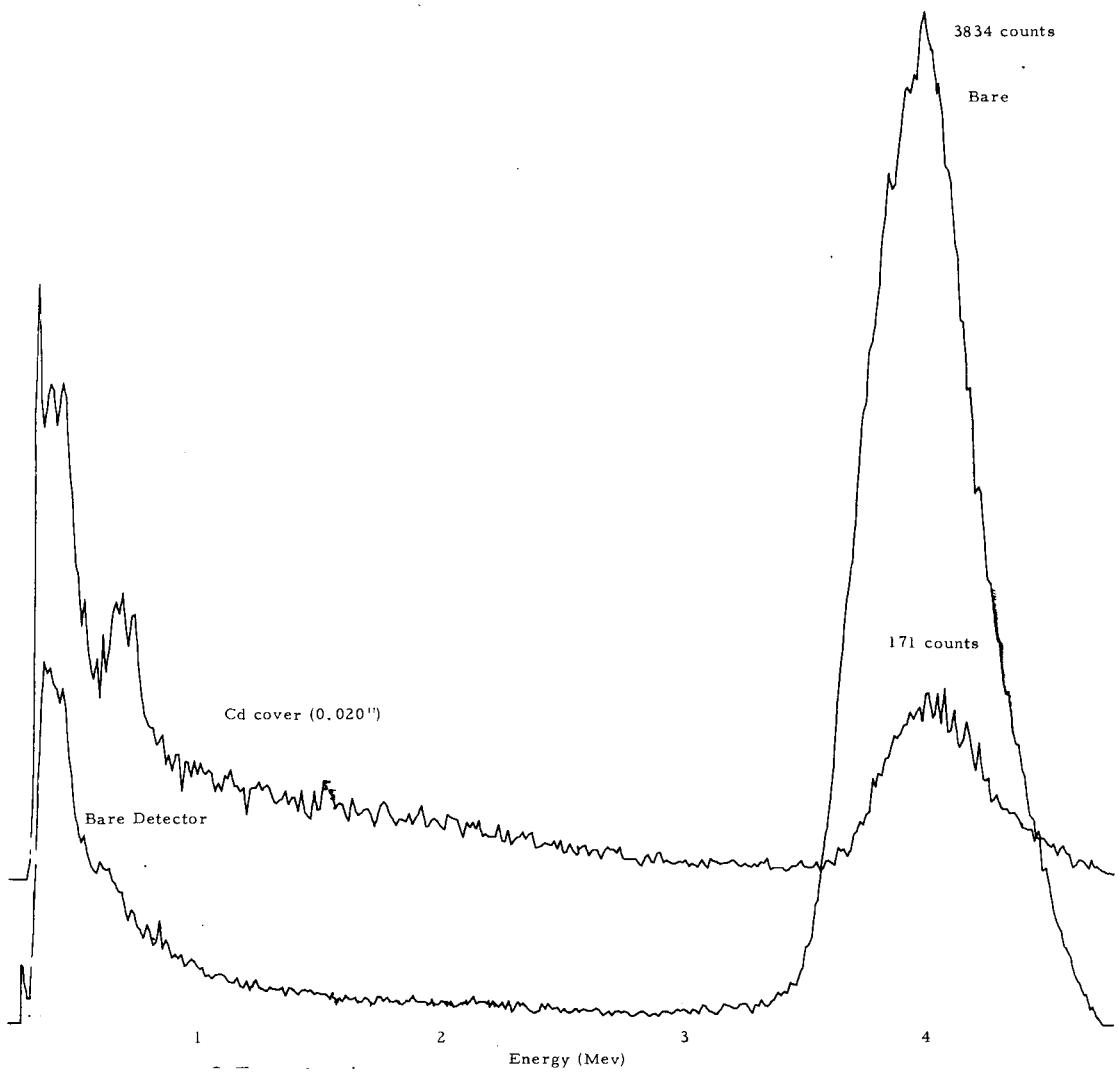

Figure 7. Output Spectrum of $Li^6I(Eu)$ Detector in Fresh Water (voltage = 880 vdc) (bare and Cd covered counts not to same scale).

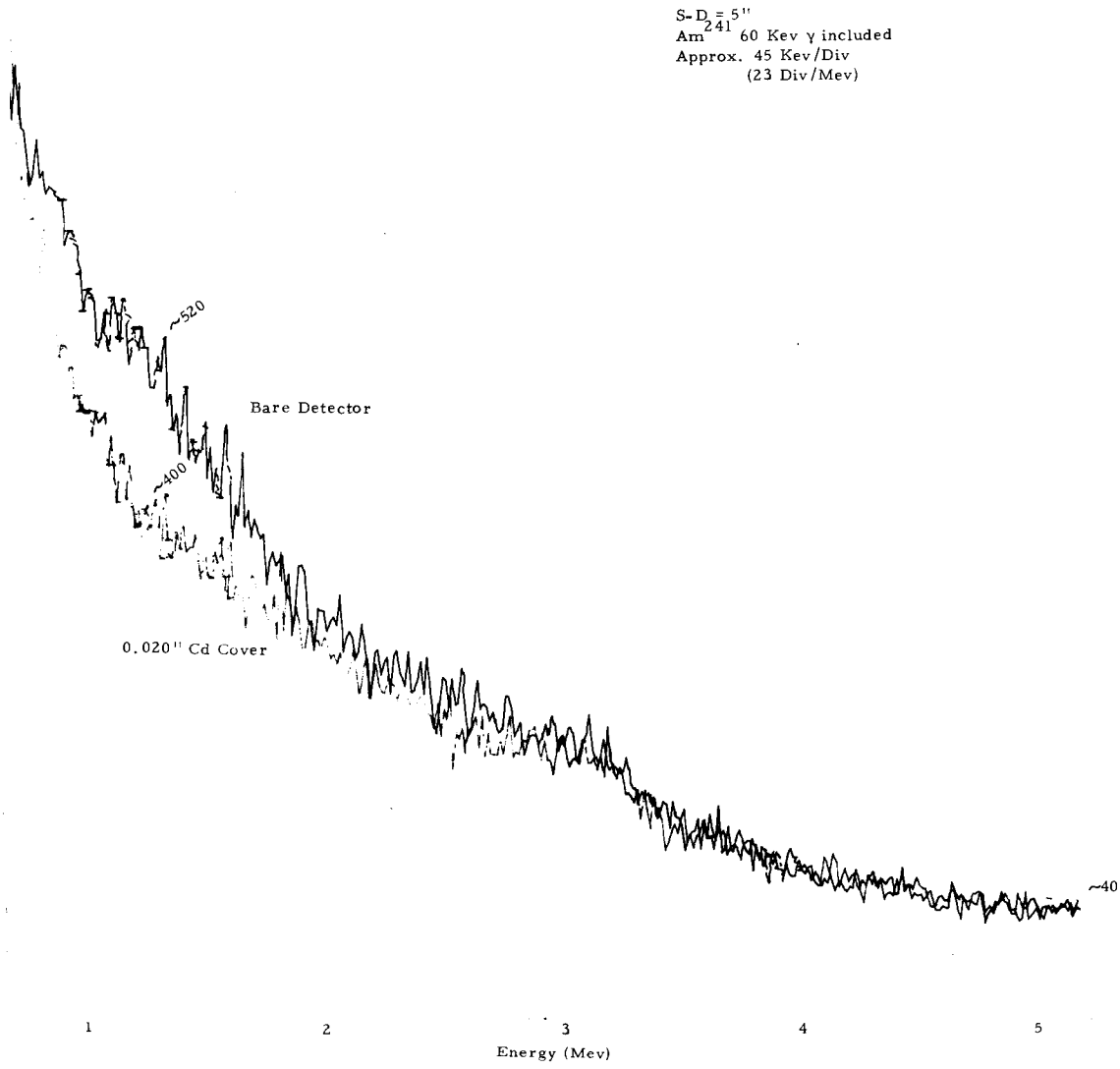

Figure 8. Output Spectrum of Gd Detector in Fresh Water (voltage = 960 vdc).

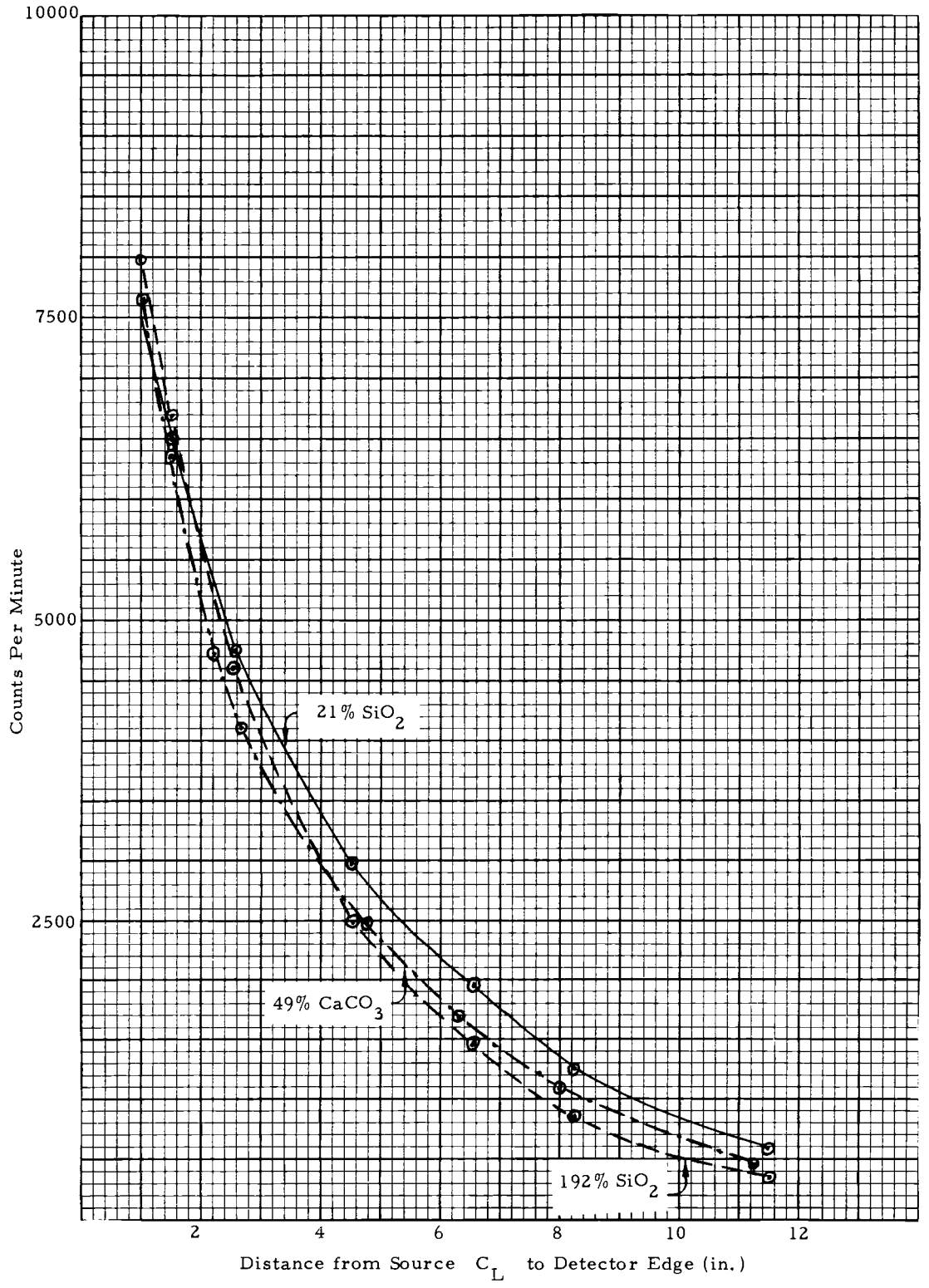

Figure 9. Variation of Epithermal Neutron Count Rate with Source-Detector Distance for LiI Detector (Cd Covered) in Zircaloy-2 Pipe.

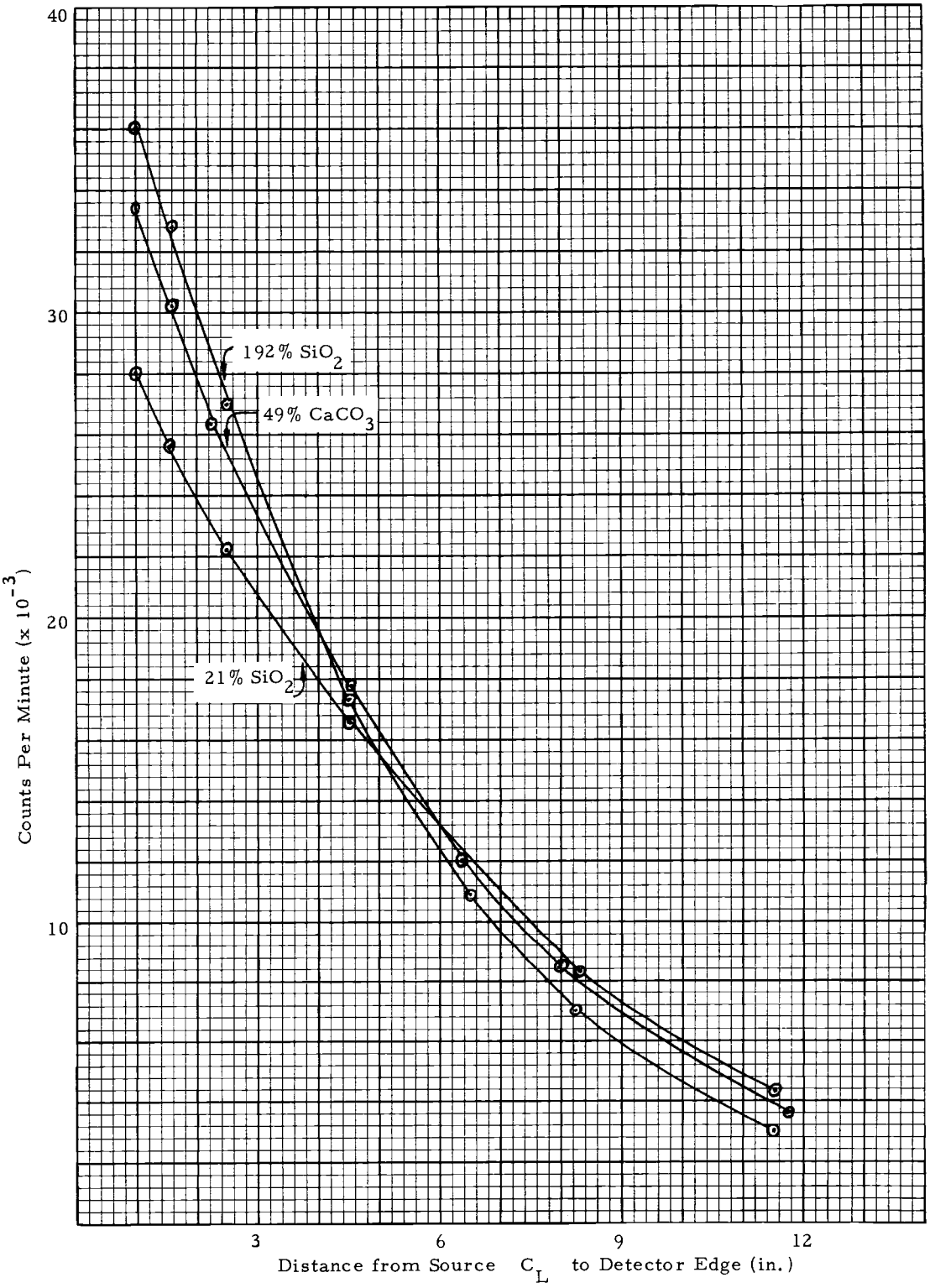

Figure 10. Variation of Thermal Neutron Count Rate with Source-Detector Distance for LiI Detector (Bare) in Zircaloy-2 Pipe.

distance for the Gd detector. These spacings should optimize the resolution among samples without undue sacrifice of total counts.

3. Effects of different container materials. Table 4 shows comparative data on the piping materials. A probe contained in zircaloy-2 showed the highest count rate; hence a zircaloy-2 container was selected for subsequent measurements.
4. Effects of temperature on the instrument. This is shown in Figure 11 for the instrument operated in tap water. Plain water was used to prevent soil parameters from masking the temperature effects.
5. Count rate versus atom percent water for various soils and detectors. These data are presented in Figures 12 through 15. Acquisition of these data were the goal of the majority of the experimental efforts.
6. Dual probe data. An attempt was made to take dual probe data even though it was felt that this type of probe would disturb the soil excessively. Count rates for the same S-D were essentially equal to single probe counts. The major problem in measurement was precise alignment of the two probes in two dimensions.

It should be noted that the six sections listed above encompassed on the order of 125 separate tests.

Table 4. Effect of Container Material on Instrument Response.

	Zircaloy-2	Aluminum	314 Stainless Steel
Bare BF_3 Detector (1 minute count)			
20% SiO_2	40264	37018	14956
25% $CaCO_3$	40350	37987	---
49% $CaCO_3$	44691	41725	---
192% SiO_2	45438	42963	15561
0.02" Cd covered BF_3 Detector (1 minute count)			
20% SiO_2	1299	1215	1195
25% $CaCO_3$	1312	1203	---
49% $CaCO_3$	1210	1144	---
192% SiO_2	1137	1082	1024
Bare LiI(Eu) Detector (1 minute count)			
20% SiO_2	28458	26612	
25% $CaCO_3$	29513	27492	
49% $CaCO_3$	33006	30513	
192% SiO_2	35847	33086	
0.02" Cd covered LiI(Eu) Detector (1 minute count)			
20% SiO_2	8080*	7633*	
25% $CaCO_3$	8073	7598	
49% $CaCO_3$	8094	7639	
192% SiO_2	8344*	7983*	

*10 minute counts

Source to detector distance for all measurements was one inch.

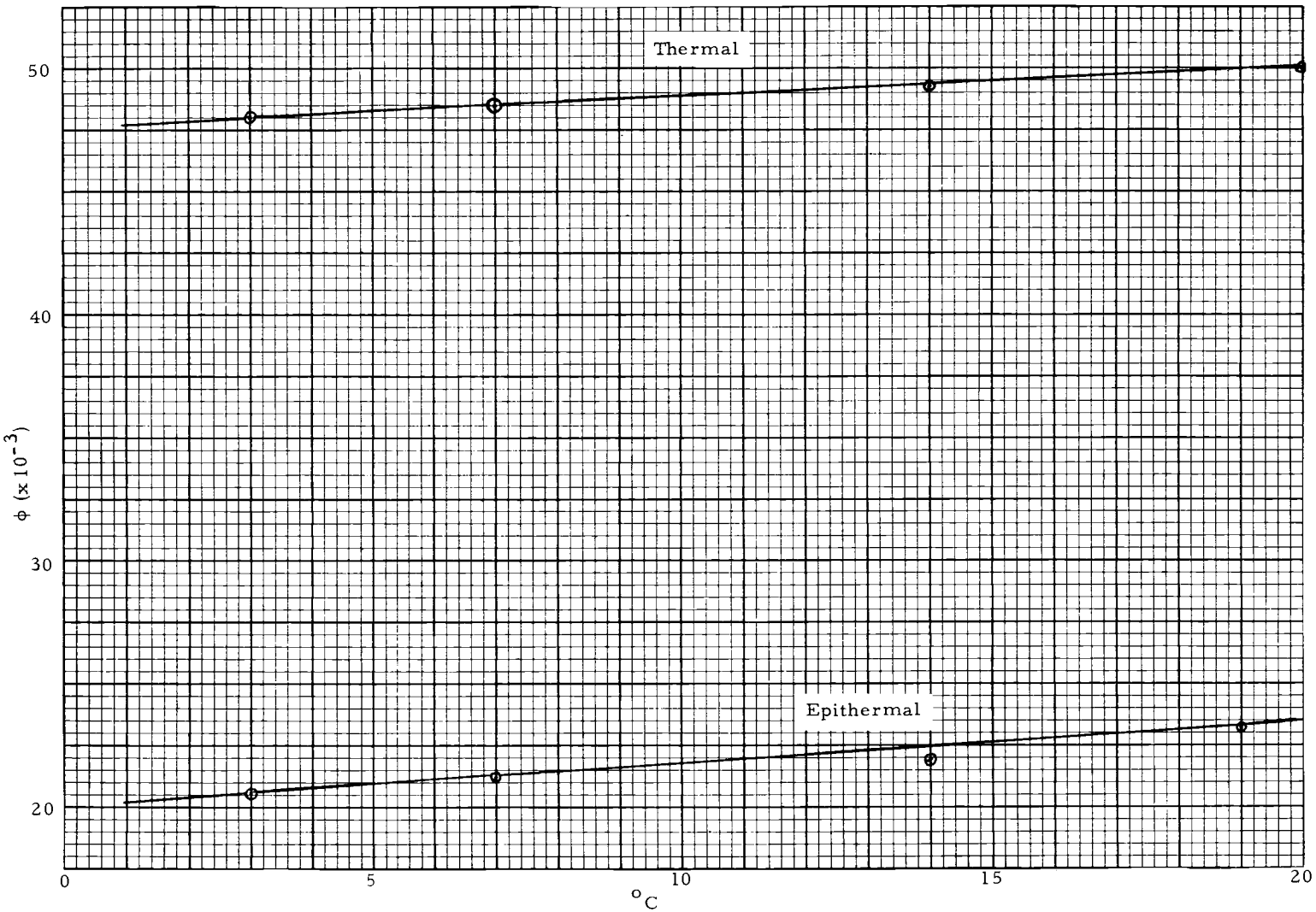

Figure 11. Variation in Count Rate with Temperature for LiI Instrument in Tap Water for Thermal and Epithermal Flux. For Thermal, $\phi \rightarrow$ counts/min. For Epithermal, $\phi \rightarrow$ counts/10 min.

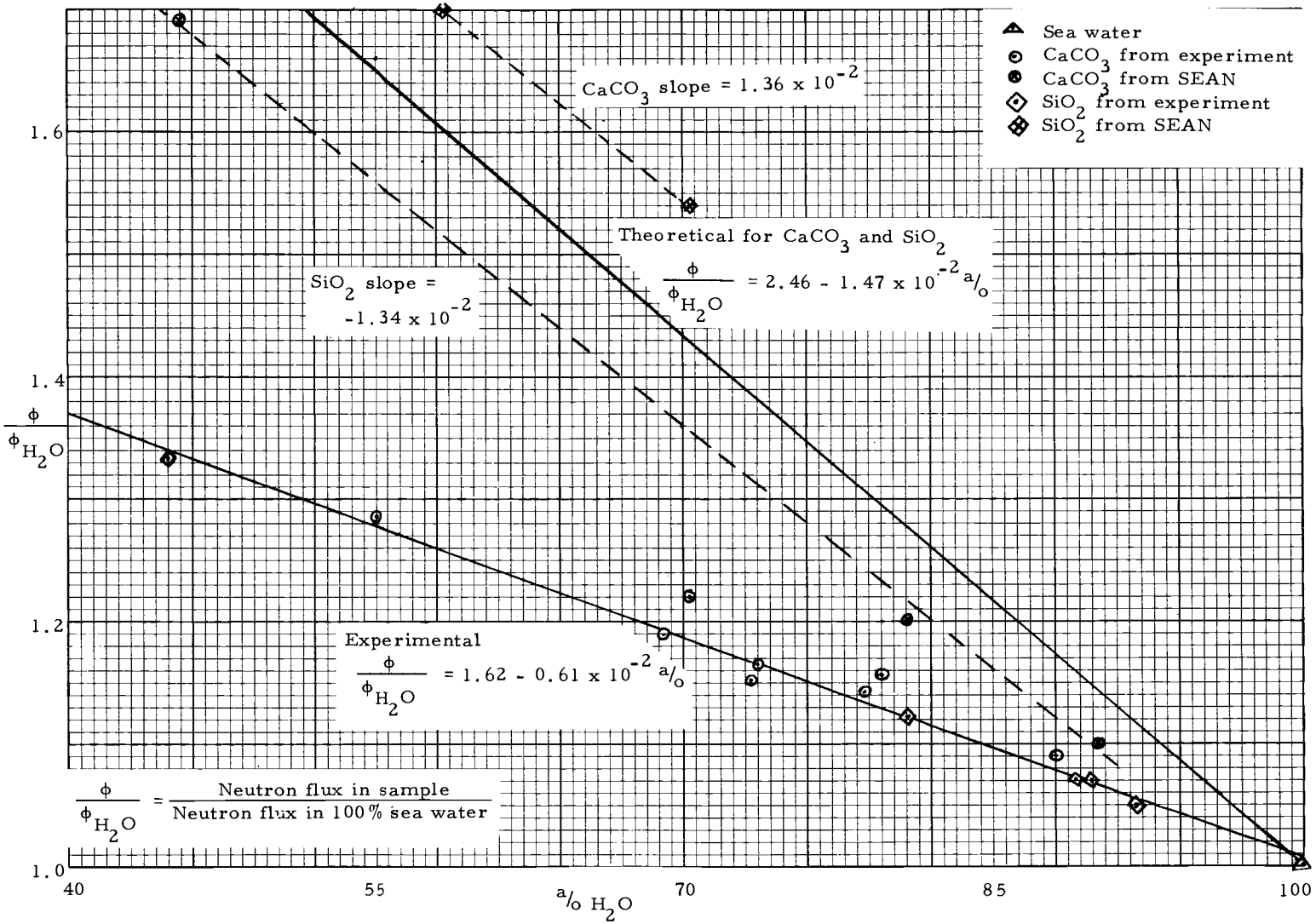

Figure 12. Epithermal Neutron Response of LiI Instrument (0.02" Cd Cover) (S-D = 5" [12.7 cm]).

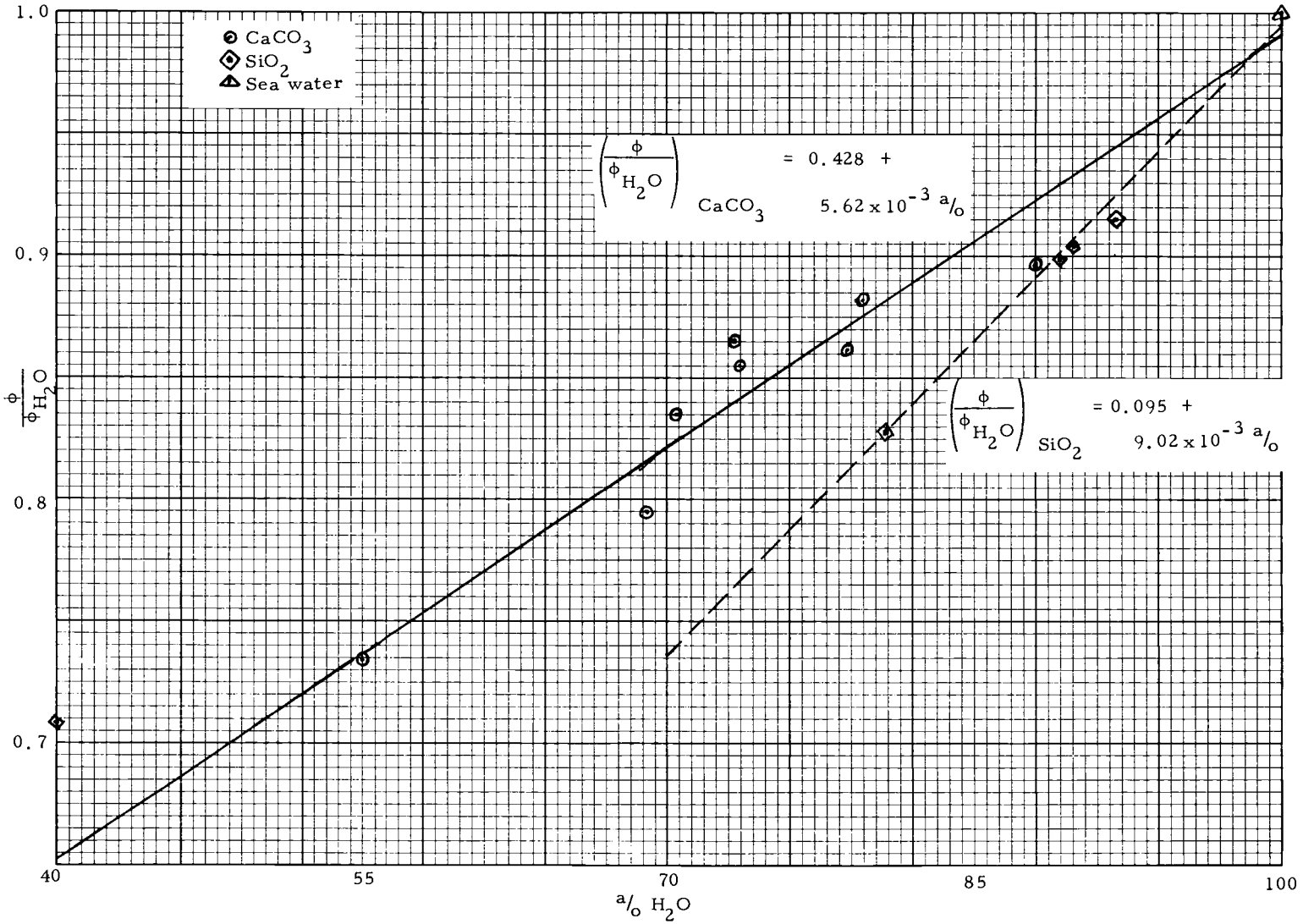

Figure 13. Thermal Neutron Response of LiI Instrument (S-D = 1" [2.54 cm]).

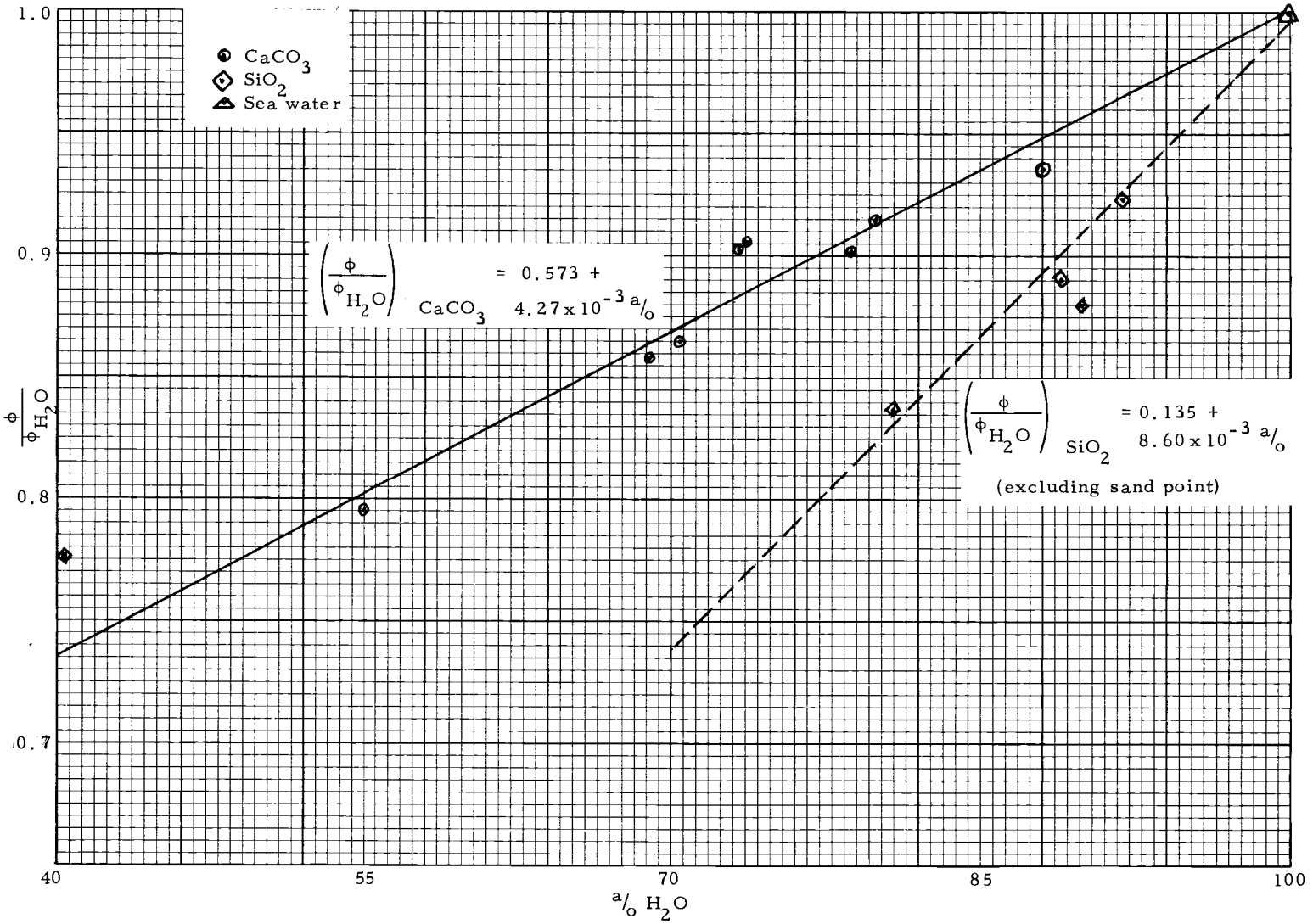

Figure 14. Thermal Neutron Response of BF_3 Instrument (S-D = 1" [2.54 cm]).

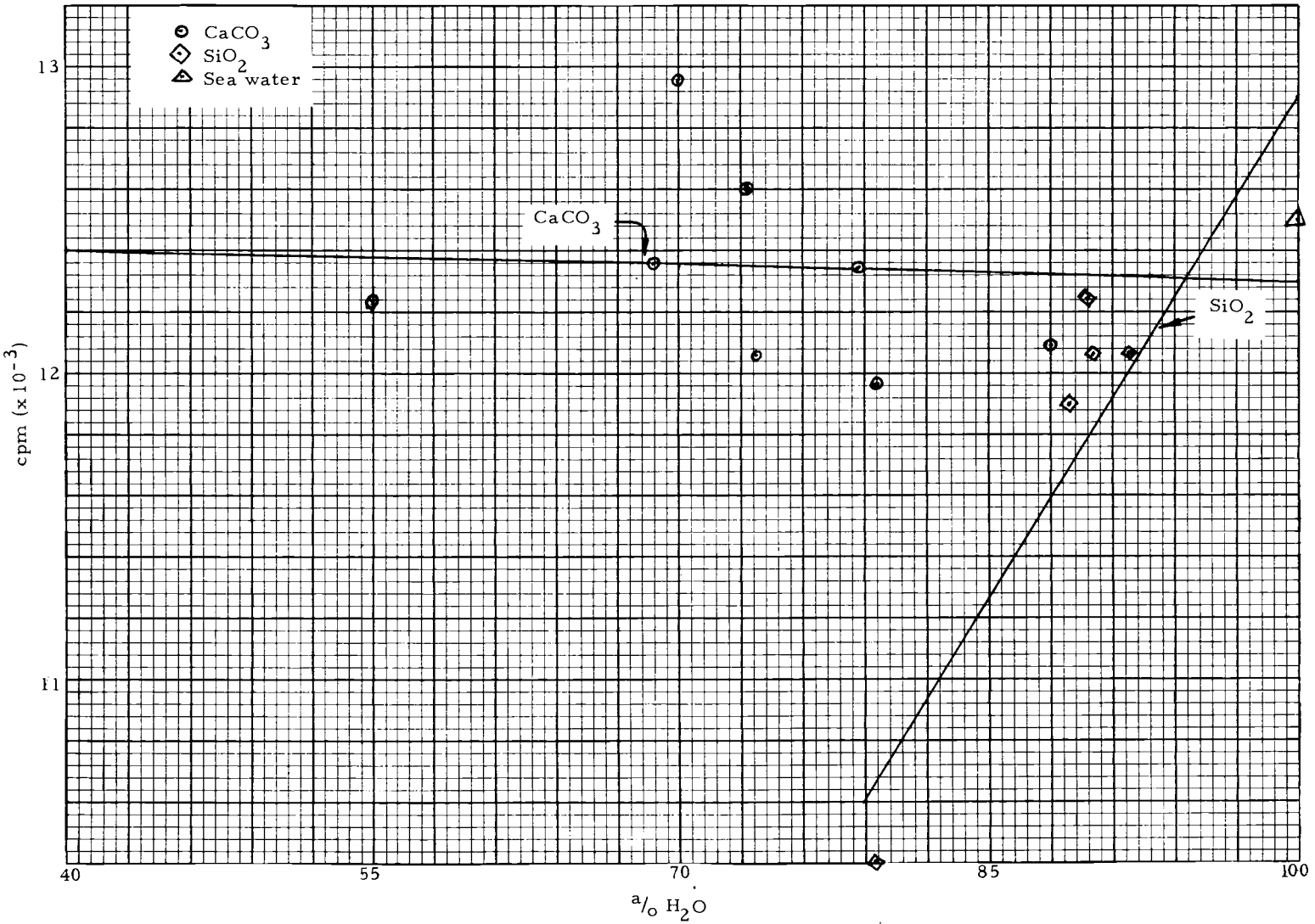

Figure 15. Response of Gd Loaded Instrument (0.02" Cd Cover) (S-D = 5" [12.7 cm]).

VI. EXPERIMENTAL PROCEDURES

Once the voltages, gains, component spacings, etc. were properly established, the calibration of the final model could be performed. This corresponds to experiment 5 of the preceding section, and was made up of three parts: mixing the samples, preparing to count the samples, and actually counting the samples.

Two methods were used in mixing samples and measuring their moisture content. For the sand samples a 55 gallon drum was positioned on a scale, weighed, and then filled with sand. Knowing the volume per unit height of the drum and then weighing its contents periodically during filling allowed calculation of the density of sand in the drum. By "dumping" scoopfuls of sand from a distance of one to three inches above the top of the sand, a loosely packed sample of density 1.56 gm/cm^3 was obtained. If the sand was poured in through a sieve or if the drum was shaken or beaten with a mallet after filling, a density of 1.77 gm/cm^3 would be obtained. A vacuum of 20 to 28 inches Hg was drawn on the drum; then sea water was introduced through a perforated ring in the bottom of the drum. This increased the density of the soil to 2.02 and 2.16 gm/cm^3, respectively. This corresponds to $w = 25.3\%$ ($a/o = 45.8\%$) and $w = 20.1\%$ ($a/o = 40.1\%$) for the two soil mixtures.

Another procedure was used for mixing the remainder of the

soils. Quantities of solids and sea water were mixed in a large rotary mixer until homogeneous to the eye and to the touch. This soil was then carefully poured or spooned into a 55 gallon drum. The weights of solid and water were recorded as a check on the moisture and density of the sample. Principal measure of the moisture content was determined from samples taken either while mixing, after counting, or at both times. The number of samples varied from three to eight. These were then baked at 105-110°C until all water had evaporated. From the weights of the samples before and after baking, the moisture content of the sample was determined. Dry samples of montmorillonite and illite were also baked to determine bound water content. This was negligible for the illite, and 9.8% at 105°C and 10.1% at 250°C for the montmorillonite.

Certain problems were encountered in the mixing process. Some materials will hold more water than others, while those "others" will mix homogeneously at low water content. Excluding the sand, the easiest samples to mix were of $CaCO_3$ (lime) and illite. Moisture contents on the order of 25% with $CaCO_3$ and 40% with illite could be mixed. Montmorillonite was very difficult to mix homogeneously, even in small batches.

Another major problem was settling. At higher moisture contents, the soils tended to settle noticably in a matter of hours. Hence readings had to be taken quickly after mixing. This did allow two sets

of data from one sample, one set taken immediately after mixing and another taken two to three days later when settling was complete.

Finally all solids, as well as the two batches of water used, were analyzed. The analyses were to determine not only their major constituents but also any other elements which, if present in any appreciable quantity, might affect neutron measurements. Most of these analyses were done by neutron activation analysis in the O. S. U. TRIGA reactor. Boron analyses were done chemically. Results of these analyses are displayed in Table 3.

Some standardization procedures were needed for the electronic equipment. Diagrams of the test circuit and data-taking circuits are shown in Figure 16. Before counting and periodically while counting, the pulse generator was used to check that the gain or discriminator setting had not changed. This eliminated any changes in electronic response with temperature and/or humidity as well as giving a constant reference which provided continuity from day to day.

It was also necessary to check the photomultiplier (PM) tube response for the LiI detector after a few months use. The gain of a PM tube changes with time and any change could subtly affect the data. Hence, the response of the system in sea water was compared with previous data and the high voltage increased as necessary. Over the whole project the voltage varied only 10 volts. Voltage adjustment was not necessary for the BF_3 since it operates on a flat voltage plateau which remains

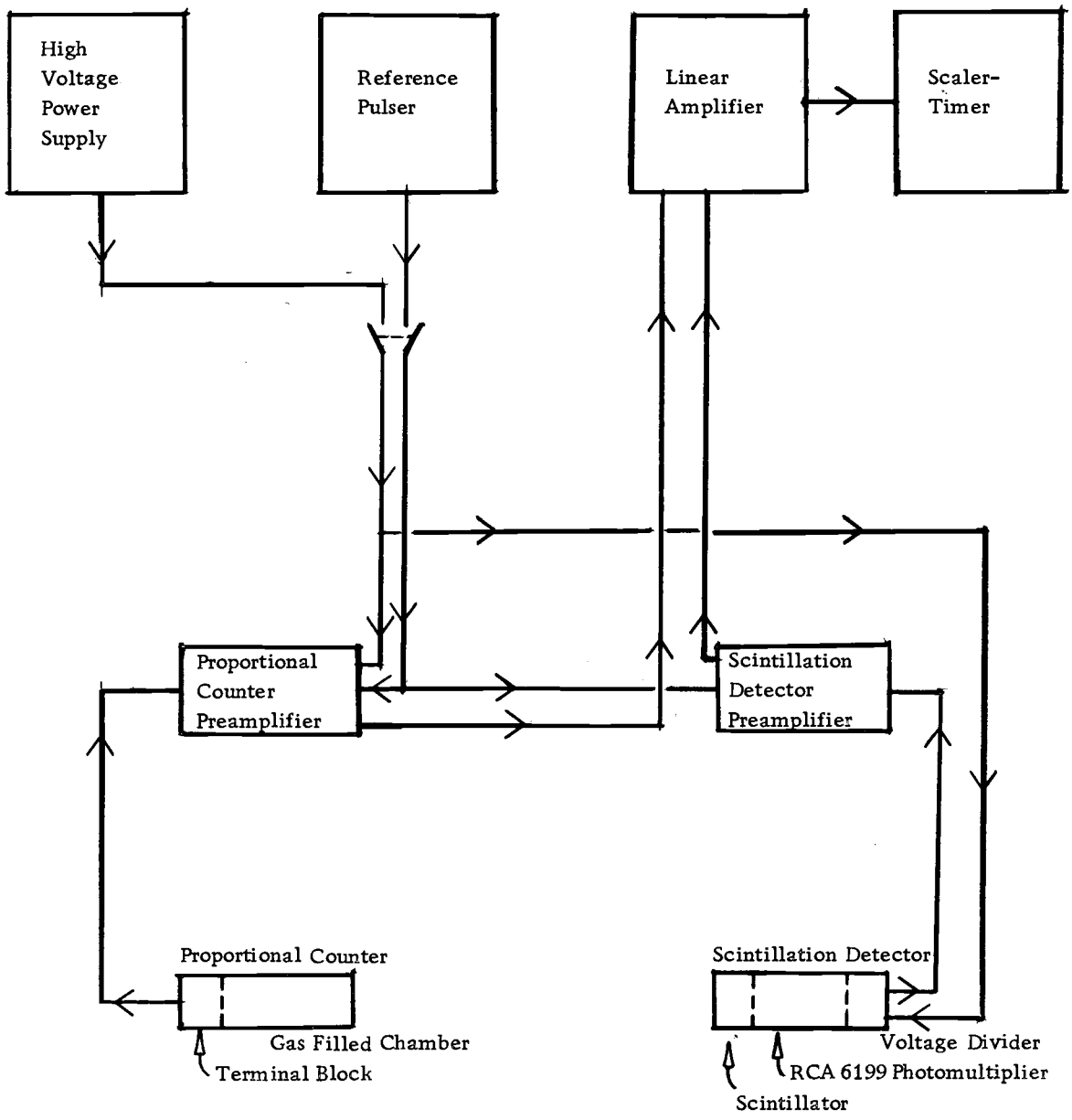

Figure 16. Block Diagram of Instrument Operating and Test Circuits (Low Voltage Power Cables Not Shown).

stable (if set correctly) over most of the life of the detector.

With proper threshold and gain settings, the residual error in this type of counting system is negligible. The minimum standard deviation is approximately equal to the square root of the total counts (2, p. 46-49). Hence one can expect accuracy on the order of a few percent for total counts over 10,000. A one minute counting time would give a total count of over 10,000 for the BF_3 detector, the Gd detector or the LiI detector sensitive to thermal neutrons. In order to ensure greater than 10,000 total counts, counting times for epithermal neutrons with the LiI detector were of ten minute duration. Fifteen one-minute counts (or three ten-minute counts for epithermal data) consistently resulted in deviations of less than two percent.

The sample size was chosen to approximate an infinite medium. The radius of the cylindrical sample was fixed by the radius of the drum less the outside radius of the pipe, or about ten inches. The height of soil was chosen so that there was at least ten inches of soil vertically between the source and any boundary. Based on a diffusion-length argument given earlier, this ensured that the model was effectively an infinite medium. This restriction was especially adhered to as water content decreased.

In addition to discriminating electronically against gamma radiation from the source, one-sixteenth inch of lead was placed over the source end of the LiI detector when counting thermal neutrons.

One-eighth inch of lead was used when counting epithermal neutrons with the LiI detector or when using the Gd detector. One-eighth inch of lead is approximately ten relaxation lengths for 60 kev γ's; hence the counts recorded were undoubtedly caused by neutrons.

VII. GENERAL DISCUSSION

As may be inferred from Figures 12 through 15, difficulties were encountered in getting reasonably solid $CaCO_3$ samples in the range of the opal and montmorillonite samples. A 133% moisture $CaCO_3$ (88 a/o water) sample finally was mixed to give some overlap; however, the sample bore more resemblance to milk of magnesia than to a solid. On the other hand, it was impossible to mix an opal or montmorillonite sample lower than 125% moisture and obtain reasonable homogeniety. Hence, each section of the calibration curve was obtained primarily with one soil type.

A possible source of error in the measurements entered through settling of the soils after mixing. To offset this, measurements were taken immediately after mixing and/or two to three days later. Still there is no way to measure settling at all points except possibly by building a container which allows sampling after the container is full. The same uncertainty enters into the amount of air in the samples. Air surely entered most of the samples during mixing. Some of the samples were placed under vacuum at points in their mixing, others had no vacuum applied; yet no difference could be noted. Fortunately, air is a problem only if large bubbles are trapped, causing irregularities in the mixture. By carefully pouring or spooning small batches into the drums, it is believed that large bubble formation was

prevented. Since both the settling and the air uncertainties raise questions about the homogeniety of the mixtures, data were often taken at three points, one and one-half inches apart in the sample. There were never any irregularities noted, suggesting that the samples were homogeneous.

Of the detectors studied or used, the $Li^6I(Eu)$ proved to be superior. It operates at 850 to 900 volts, yet can produce the high count rates noted in Table 4 with a crystal size one-half inch in diameter and one-half inch long. Hence it is a good approximation to a point detector. It adapts easily to either epithermal or thermal neutron counting and could also be used as a gamma detector. Only two disadvantages of LiI were noted. Due to LiI being highly hygroscopic, the crystal and PM tube are a hermetically sealed unit and should be replaced by the vendor if it ever becomes necessary. Also, as mentioned earlier, the gain of the PM tube can change with age, so if data are to be correlated over long periods of time for different absolute counts, a reference must be set up and maintained.

The BF_3 detector is a good thermal neutron detector with a very stable voltage plateau. However, it is far too large to be useful as a point detector. Its size causes the response to be an "average" over a large area, hence thin layers which may exist in the sediment would be smeared out and never seen as such. When both detectors are covered with cadmium, the BF_3 output is only about one-eighth

that of the LiI detector. The Gd detector could be a good inexpensive thermal neutron detector. It is larger than the LiI, being 1" O.D. x 1" O.L., yet still considerably smaller than the BF_3. Without a cadmium cover, its count rate was of the same order of magnitude as that of the BF_3. Unfortunately, the detector will be unsatisfactory as an epithermal detector until a method of differentiating between the capture γ's from the cadmium cover and epithermal neutrons is developed. A possibility would be to cover the Gd detector with a non-γ emitter such as boron or a boron compound. In any case, this would be a project in itself.

A drawback of the present system is the ten minute counting time necessary for good accuracy in epithermal neutron counting. This could be shortened by increasing the source strength by a factor of ten, since the flux and the count ratios are directly proportional to the source strength. This would also necessitate more shielding of the source when not in use as described below.

As discussed in the section on electronics, the system could also be operated with a single channel analyzer and analog stabilizer, thus counting all the pulses in an energy interval, rather than all the pulses above a certain energy. If this differential method is used, the system becomes sensitive to shifts in the mean energy of pulses with changes in water content. Although a very slight effect in an (n, α) detector, it would necessitate a wide window to ensure the

proper moisture range for the instrument. Using a threshold below the neutron pulse peak (as has been done) gives virtually the same result with two less pieces of equipment. This is possible because of the negligible number of neutrons or γ's in this system having energies greater than the 4.78 Mev given off by the Li^6 (n, α) He^3 reaction.

One of the most pleasant aspects of this project has been the minimal radiological problems. The 89 millicurie (mCi) AmBe source is convenient to handle and simple to store. As shown in the photographs, the source slipped neatly into an aluminum holder which threaded onto a rod, and this in turn screwed into the end of the detector assembly. The source was handled for less than a minute while being attached or disconnected from the detector. When not in use, it is stored in an eight inch steel container filled with paraffin.

Gamma, fast neutron, and thermal neutron dose rates were frequently monitored whenever the source was exposed. The dose rate at the surface of the source holder totaled 500 mrem/hr of neutron and γ radiation. At the surface of the paraffin-filled source container, the dose rate dropped to 5 mrem/hr. To obtain an upper limit on the dose rate a person handling the source could expect to encounter, the source in its holder was positioned against a film badge and left for 15 minutes. The film indicated 440 mrem/hr from

neutron radiation and 80 mrem/hr from γ radiation. All personnel involved in the research wore β - γ-neutron film badges at all times. The highest total recorded exposure for any one person working on the project was 10 mrem.

The dose rates observed in handling this source indicate that source strength could be increased by a factor of ten without involving serious radiological hazards. Dose rate is approximately linear with source strength; hence most of the measured dose rates above would increase by about a factor of ten.

Figure 11 shows the effect of temperature on the instrument. No attempt was made to determine which components of the system were most affected by temperature change. Compensation for temperature variation can be accomplished by correcting the output for temperature if the sea floor temperature is known, or by suspending the probe just above the ocean floor and adjusting the gain to give a reading equal to that of sea water at the instrument calibration temperature. Since the probe will be sealed, changes in pressure should not be felt by the detector, and no pressure corrections should be necessary. Correction for the compressibility of water at great depths is inherently included with the temperature effect gain adjustment made before entering the marine sediment.

Figures 12 through 15 show the relationship between atom percent water ($^{a}/_{o}$) and count rate (CPM). As can be seen from Figure

15, the Gd detector data are useless. More work needs to be done in determining the proper source-detector distance. Hence, further discussion will exclude the Gd detector data.

The LiI epithermal neutron data of Table 5 are displayed as Figure 12. This exhibits a linear relationship between $^{a}/_{o}$ and CPM which is independent of the solid material parameters for the water content region of interest. The equation of this line, obtained by a linear least-square fit, is

$$\frac{\phi}{\phi_{H_2O}} = 1.62 - 0.00611\ ^{a}/_{o} \qquad \text{(VII-1)}$$

where

$\frac{\phi}{\phi_{H_2O}}$ is the ratio of the sample CPM to the CPM in sea water.

Table 12 also displays the analytical solution generated by SEAN for typical soils. It is apparent the slopes of the SEAN-generated lines and the experimental line differ. This is due to SEAN considering only the epithermal neutron flux, while the LiI detector transmits not only epithermal neutron absorption, but also the electronic and radiation background signal shown in Figure 7. Of more importance, the SEAN curves are straight lines with slopes of the same order of magnitude as the experimental curve.

Table 5. Epithermal Neutron Counting Data (LiI Detector with S-D = 5 inches).

a/o	Moisture	Sediment	Counts Per 10 Min	$\frac{\phi}{\phi_{H_2O}}$
40.4	20.3	Sand	32300±180	1.370
45.8	25.5	Sand	31381±177	1.330
55.0±0.0	22.0± 0.7	$CaCO_3$	30385±174	1.285
69.0±0.02	40.0± 3.3	$CaCO_3$	28265±168	1.195
70.4±0.00	42.7± 0.9	$CaCO_3$	28779±408	1.220
73.4±0.00	49.6± 1.0	$CaCO_3$	27305±432	1.155
73.6±0.00	50.4± 1.0	$CaCO_3$	27468±166	1.165
78.8±0.00	66.9± 1.5	$CaCO_3$	26859±173	1.140
(78.8)*	64.1± 0.4	Illite	26813±164	1.135
79.6±0.01	70.2± 3.1	$CaCO_3$	27283±165	1.155
80.8±0.00	125.9± 3.9	Opal	26490±163	1.120
(82.1)*	126.1± 3.9	Mixture**	26377±253	1.115
(87.0)*	177.4±11.1	Montmorillonite	25596±223	1.085
88.0±0.00	131.9± 4.9	$CaCO_3$	25761±168	1.090
89.0±0.00	243.2± 4.5	Opal	25336±264	1.070
89.9±0.00	246.5± 1.1	Opal	25281±534	1.070
91.9±0.00	339.6± 1.2	Opal	24806±256	1.050
(96.9)*	441.0±37.6	Montmorillonite	24189±219	1.025
100	∞	Sea Water	23604±236	1.000

*Values in parentheses are a/o's read from Figure 12.

**Mixture was 60% $CaCO_3$, 10% SiO_2, 30% Montmorillonite.

The thermal neutron data obtained with the LiI and BF_3 detectors are given in Table 6 and shown in Figures 13 and 14. These display a linear relationship between $^a/_o$ and CPM for both the LiI and BF_3 detectors. Again the data were fit to a linear-square approximation. For each soil, the equation of the LiI line is:

$$\frac{\phi}{\phi_{H_2O}} = 0.428 + 0.00562\ ^a/_o \quad \text{for } CaCO_3$$

$$\frac{\phi}{\phi_{H_2O}} = 0.095 + 0.00902\ ^a/_o \quad \text{for } SiO_2 \qquad \text{(VII-2)}$$

while for the BF_3 data:

$$\frac{\phi}{\phi_{H_2O}} = 0.573 + 0.00427\ ^a/_o \quad \text{for } CaCO_3$$

$$\frac{\phi}{\phi_{H_2O}} = 0.135 + 0.00860\ ^a/_o \quad \text{for } SiO_2 \qquad \text{(VII-3)}$$

The SiO_2 lines do not include the sand data point at 40.4 $^a/_o$ since the compositions of the sand and opal differ such that their thermal neutron cross sections will be appreciably different. It might be noted that Eqns. (VII-2) and (VII-3) are very similar.

Due to the dependence of w on the mass (weight) of solids, the instrument could not be calibrated to read w directly. For instance, 88 $^a/_o$ corresponds to 123% moisture in $CaCO_3$ while 89 $^a/_o$ corresponds to 243% moisture in SiO_2. Hence w must be

Table 6. Thermal Neutron Counting Data (S-D = 1 inch).

a/c	Moisture	LiI CPM	$\frac{\phi}{\phi_{H_2O}}$	BF_3 CPM	$\frac{\phi}{\phi_{H_2O}}$
For $CaCO_3$					
55.0	22.0	30338±191	0.733	42153±224	0.795
69.0	40.0	32941±154	0.795	45452±180	0.857
70.4	42.7	34509±119	0.834	46902±212	0.885
73.4	49.6	35832± 47	0.865	47812±309	0.902
73.6	50.3	35323±152	0.853	48020±164	0.906
78.8	66.9	35721±174	0.862	47806±191	0.902
79.6	70.2	36500±211	0.882	48369±219	0.914
88.0	131.9	37168±130	0.896	49476±254	0.934
For SiO_2					
40.4	20.3	29300±171	0.707	41000±410	0.774
45.8	25.5	--		--	
80.8	125.9	34252±185	0.827	44291±211	0.836
89.0	243.2	37194±116	0.898	47156±204	0.891
89.9	246.5	37394± 10	0.904	46068±241	0.879
91.9	339.6	38309±200	0.925	48964±280	0.924
For Sea Water					
	∞	41407±203	1.0	53032±530	1.0
For Illite					
	64.1	33393±105	0.806	--	--
For Montmorillonite					
	176.5	38322±255	0.925	50789±196	0.958
	441.0	40543±170	0.978	51615±516	0.974
For 60% $CaCO_3$, 10% Opal, 30% Montmorillonite Mixture					
	126.1	38606±385	0.932	51126±511	0.966

determined indirectly.

The results shown in Figure 12 coupled with a knowledge of the soil density can be used to give an in situ measurement of w. This is shown by Eqn. (II-28).

$$w = \frac{a/o}{\rho - 0.01\, a/o}$$

It will be noted that Eqn. (II-28) presupposes no knowledge of solids type.

As discussed earlier, a dual probe instrument is considered unsatisfactory because of the disturbances in the ocean floor that two probes spaced relatively close together would make. Also there is the physical problem of keeping the probes equally spaced. To obtain enough counts to ensure good accuracy in a reasonable length of time, it is necessary to place the detector and source no more than six inches apart. This distance could be increased by increasing the source strength; this not only increases the radiological handling problems, but a larger S-D distance also reduces the response of the instrument to local changes in water content.

The source-detector distances as well as the effective sphere of influence of the probe are dependent on the diffusion length. Up to about three diffusion lengths from the source, the count rate will decrease as the amount of water decreases, for the lower water content corresponds to a larger L. For S-D greater than about 3L,

the count rate decreases with increasing water content simply because fewer neutrons reach the detector. A larger S-D allows better resolution between data points. However, the final S-D is a compromise; for as S-D increases, the count rate for any water content decreases. Hence the S-D of five inches for epithermal neutrons and one inch for thermal neutrons is a compromise between adequate count rate and resolution.

Sphere of influence is defined as "the more or less spherical zone of the medium, which effectively contributes to the observed activity of the detector" (5, p. 15). This essentially defines the radius of soil around the source necessary to have an infinite medium. Since L is a measure of the attenuation of ϕ with distance, the instrument's sphere of influence for a given soil will increase as the diffusion length increases.

The solids-independent linear variation of count rate with $^{a}/_{o}$ for epithermal flux greatly simplifies future calibration efforts. At worst, two samples of different moisture content would be required. Calibration in conjunction with the results of the numerical solution could allow a one-point calibration. These samples could be made with anything which would mix with water, including marbles, concrete or soil solids.

The ultimate worth of the probe design and calibration procedures outlined above will be determined by the accuracy with which

a/o can be determined and with which the moisture can be related to the a/o. As noted in Table 5, the accuracies in counts are on the order of 1 to 2%. The accuracies in a/o of the samples are consistently less than that. This gives a standard deviation in any measurement of about 2.5%. From Eqn. (II-28) the deviation in w corresponding to deviations in density and water content is given by

$$q_w = \frac{1}{\rho - 0.01\, a/o} \sqrt{\rho^2 q_{a/o}^2 + (a/o)^2 q_\rho^2} \qquad \text{(VII-4)}$$

This gives a fractional error of

$$\frac{q_w}{w} = \frac{\sqrt{\rho^2 q_{a/o}^2 + (a/o)^2 q_\rho^2}}{a/o} \qquad \text{(VII-5)}$$

As an example, for $q_\rho = 0.1$, $q_{a/o} = 2.0\%$ $\rho = 1.3$, and $a/o = 80\%$

$$\frac{q_w}{w} = \frac{8.4}{80} = 10.5\%$$

Both q_ρ and $q_{a/o}$ are extreme values, so the fractional error should normally be much lower than 10%.

If the density of the solid (ρ_s) in the soil is known, w can be determined from a density measurement alone.

$$\rho = \frac{m_{solid}(1 + \frac{w}{100})}{\frac{m_{solid}}{\rho_s} + (\frac{m_{solid}}{\rho_{H_2O}})(\frac{w}{100})}$$

$$\rho = \rho_s \frac{(1 + \frac{w}{100})}{(1 + \frac{w\rho_s}{100})} \qquad \text{(VII-6)}$$

$$w = \frac{100(\rho_s - \rho)}{\rho_s(\rho - 1)} \qquad \text{(VII-7)}$$

and

$$\frac{q_w}{w} = \frac{1}{100\rho_s(\rho_s - \rho)(\rho - 1)} \left[\rho^2(\rho-1)^2 q_{\rho_s}^2 + 10^4 \rho_s^2 (1-\rho_s)^2 q_\rho^2\right]^{\frac{1}{2}} \qquad \text{(VII-8)}$$

Using Eqns. (VII-6) and (II-28), $w(^a/_o, \rho_s)$ can be determined by solving the resulting quadratic equation. This is

$$w = \frac{^a/_o}{\rho_s(1-0.01\,^a/_o)} \qquad \text{(VII-9)}$$

and

$$\frac{q_w}{w} = \frac{\left[^a/_o{}^2(1-0.01\,^a/_o)^2 q_{\rho_s}^2 + \rho_s^2 q_{^a/_o}^2\right]^{\frac{1}{2}}}{^a/_o\,\rho_s(1-0.01\,^a/_o)} \qquad \text{(VII-10)}$$

Table 7 shows the results of the aforementioned methods for three samples. Method (1) corresponds to Eqn. (II-28), method (2) to Eqn. (VII-6), and method (3) to Eqn. (VII-9). The samples are montmorillonite, illite, and a 60% $CaCO_3$-10% SiO_2-30% montmorillonite mixture. ρ_s was assumed to be 2.7 gm/cm^3 in all cases with $q_{^a/_o} = 3\%$ and $q_\rho = q_{\rho_s} = 0.1$ gm/cm^3.

As will be noted, the errors in Table 7 are very high, even for method (1) which uses two measured quantities. However, the

Table 7. Comparison of Moisture Content Measurements.

Measurement	64% Illite	126% Mixture*	177% Montmorillonite
Method (1)	76.1± 9.6%	117.1±13.8%	191.2±19.1%
Fractional Error (1)	18.8%	7.1%	8.0%
Method (2)	44.2±10.5%	84.1±23.3%	157.2±44.8%
Fractional Error (2)	31.2%	33.3%	11.3%
Method (3)	137.7±25.2%	168.7±34.9%	247.9±66.4%
Fractional Error (3)	115.1%	33.9%	73.0%
By Baking	64.1± 0.4%	126.1± 3.9%	177.4±11.1%

*Mixture was 60% $CaCO_3$, 10% SiO_2, 30% Montmorillonite

Method (1): $$w = \frac{a/o}{\rho - 0.01\, a/o} \qquad \text{(II-28)}$$

Method (2): $$w = \frac{100\,(\rho_s - \rho)}{\rho_s(\rho - 1)} \qquad \text{(VII-7)}$$

where $\rho_s = 2.7$ regardless of the solid in the soil

Method (3): $$w = \frac{a/o}{\rho_s(1 - 0.01\, a/o)} \qquad \text{(VII-9)}$$

$q_\rho = q_{\rho_s} = 0.1\ \text{gm/cm}^3 \qquad q_{a/o} = 3\%$

information is not presented to display the great accuracy of any method, but merely to point out the effects of using a given method. Some of the error shown in the table is due to uncertainties in our density measurements and to the assumptions used in obtaining Eqn. (II-28). Due to water standing on top of the samples, it was very difficult to accurately determine the volume of sample. Some sample weight was lost in sample preparation and through evaporation; however, this was probably negligible in comparison to the total weight of soil. In any case, the instrument will determine moisture content when coupled with a density measurement. Which method to be used and the accuracy desired will be determined by the particular investigator. Then the error will be strictly dependent on the care exercised in calibration of the moisture and/or density meter.

VIII. CONCLUSIONS AND DESIGN SPECIFICATIONS

A nuclear moisture meter can be constructed utilizing epithermal neutrons to measure water content in atom percent without knowledge of the sediment constituents. Design specifications are given below.

When used in conjunction with some form of density measurement, the percent moisture (w) can be determined in situ. The accuracy of this determination depends on the accuracy of calibration of both measuring devices.

Instrument design specifications are:

Source -- $Am^{241}Be$ emitting 2×10^5 to 2×10^6 n/sec

Detector -- 1/2" diameter x 1/2" thick $Li^6I(Eu)$ crystal surrounded by 0.02" cadmium and with 0.125" lead between the source and detector. The crystal will be mounted on a RCA 6199 photo tube with voltage divider mounted in the detector. The whole assembly should be less than 3" O.D. and 12" O.L.

Electronic equipment -- As given in Table 2. All but the preamplifier should be above water level.

Probe construction -- a single zircaloy cylinder sealed at the source end with a hemisphere and at the connection end by a flat plate. It should be about 18 to 20 inches in length.

Source to Detector Distance -- approximately five inches.

Calibration of the instrument is critical. Some suggestions to improve accuracy in initial laboratory calibration are:

(1) Construct a sample drum of transparent material such that samples of the soil could be taken while measurements are in progress.

(2) Take measurements only after the material has settled completely. High moisture content data can be replaced by data from pure sea water.

(3) Three very precise data points should set the calibration curve. A pure sea water, an ~85% opal and a 40 to 50% $CaCO_3$ sample are suggested.

(4) Establish a distilled water standard to ensure a constant photomultiplier tube output through periodic high voltage adjustments.

(5) If possible, use a large mixer to prepare samples in the drum in which they will be measured. This eliminates soil transfers and hence weight loses which can affect density calculations.

If the instrument is initially well calibrated, future calibration checks should involve little more than a one point calibration in the distilled water sample, and then a gain adjustment for temperature just before the probe enteres the sediment.

BIBLIOGRAPHY

1. Argonne National Laboratory. Reactor physics constants. 2d ed. Washington, D. C., 1963. 850 p. (U. S. Atomic Energy Commission. ANL-5800)

2. Beers, Yardley. Introduction to the theory of errors. 2d ed. Reading, Massachusetts, Addison-Wesley, 1957. 66 p.

3. Lamarsh, John R. Introduction to nuclear reactor theory. Reading, Massachusetts, Addison-Wesley, 1966. 585 p.

4. Meghreblian, Robert V. and David K. Holmes. Reactor analysis. New York, McGraw-Hill, 1960. 808 p.

5. Moerman, P., M. DeBoodt and P. Mortier. The spatial resolution of the neutron moisture meter. In: Soil-moisture and irrigation studies: Proceedings of a panel on the use of isotope and radiation techniques in soil-moisture and irrigation studies organized by the Joint FAO/IAEA Division of Atomic Energy in Food and Agriculture, Vienna, 1966. Vienna, International Atomic Energy Agency, 1967. p. 15-20.

6. Price, William J. Nuclear radiation detection. 2d ed. New York, McGraw-Hill, 1964. 430 p.

7. Smith, P. E. et al. The use of nuclear meters in soils investigations: a summary of worldwide research and practice. Philadelphia, American Society for Testing and Materials, 1968. 136 p. (ASTM STP 412)

8. Wilson, Billy F. and Arthur H. Youmans. A sediment porosity meter: a feasibility study. Houston, Lane-Wells Company, 1966. 67 p. (U. S. Atomic Energy Commission. ORO-3325-1)

APPENDICES

APPENDIX I

Explanation of Symbols

A_{H_2O}	atomic weight of water (gm/mole)
A_{solid}	atomic weight of solid (gm/mole)
$a/_o$	atom percent water (%)
D	neutron diffusion coefficient (cm)
E	energy (eV)
G	number of discrete energy groups
$\vec{J}$	neutron current density (neutron/cm^2-sec)
L	neutron diffusion length (cm)
m	mass (gm)
m_{H_2O}	mass of water (gm)
m_{solid}	mass of solid (gm)
n	neutrons per unit volume (neutron/cm^3)
N_{H_2O}	number density of water (molecules/cm^3)
$N^0_{H_2O}$	number density of pure water (molecules/cm^3)
N_i	number density of i^{th} type atom or molecule (atoms or molecules/cm^3)
N_0	Avogadro's number (6.023×10^{23} atoms or molecules/mole)
N_{solid}	number density of solid (molecules/cm^3)

$q_{a/o}$	standard deviation from the mean value of a/o (%)
q_w	standard deviation from the mean value of w (%)
q_{ρ_s}	standard deviation from the mean value of ρ_s (gm/cm^3)
q_ρ	standard deviation from the mean value of ρ (gm/cm^3)
s	neutron source strength ($neutron/cm^3$-sec)
V_{H_2O}	volume of water in system (cm^3)
$V^0_{H_2O}$	effective volume of a single water molecule (cm^3)
V^0_{solid}	effective volume of a molecule of solid (cm^3)
V_{total}	total volume of system (cm^3)
w	moisture content (%)
α	alpha radiation
β	beta radiation
γ	gamma radiation
$\bar{\mu}$	average of the cosines of the neutron scattering angles for a particular element as molecule
ρ	density of soil or sediment (gm/cm^3)
ρ_s	density of solid (gm/cm^3)
σ_a	microscopic absorption cross section (b) (one barn (b) = 10^{-24} cm^2)
σ_s	microscopic scattering cross section (b)

σ_T	total microscopic cross section (b)
Σ_a	macroscopic absorption cross section (cm^{-1})
Σ_r	macroscopic removal cross section (cm^{-1})
Σ_s	macroscopic scattering cross section (cm^{-1})
Σ_T	total macroscopic cross section (cm^{-1})
ϕ	flux (neutrons/cm^2-sec)
$\frac{\phi}{\phi_{H_2O}}$	neutron flux/neutron flux in pure sea water

APPENDIX II

Listing of Program SEAN

```
      PRØGRAM SEAN
C     THIS SØLVES THE 4-REGIØN EIGENVALUE EQUATIØN FØR A
C     10-GRØUP,1-DIMENSIØNAL SYSTEM IN ANY GEØMETRY.  PERPENDICULAR
C     BUCKLING MAY BE INCLUDED IN THE ABSØRPTIØN TERM.
      DIMENSIØN AN(10,201),B(201),BC(4),BN(10,201),C(201),
     CCN(10,201),D(10,4),DH(10,4),DR(4),FE(10,201),FN(10,201),
     CH(4),N(4),RP(201),R(201),S(10,4),SC(10,10,4),SR(10,4),
     CTØT(10,4),SLØW(4,201),VL(201),VR(201),Z(201),BP(4),ITITLE(4)
      INTEGER P,PP,G,RG,RF
      READ(40,19)NØ
      READ(40,19)M,P,RG,NP,MS1,MS2
      RF=RG-1
      NJ=NØ-1
      READ(40,18)(BP(I),I=1,RG)
      READ(40,18)(BC(I),I=1,RG)
      READ(40,19)(N(I),I=1,RF)
24    READ(40,6)ITITLE
      IF(ITITLE.EQ.3HEND)GØ TØ 25
      DØ 9 J=1,RG
      DØ 7 I=1,M
      READ(40,8)D(I,J),SR(I,J)
      IF(J.LE.MS1.AND.I.LE.MS2)READ(40,8)S(I,J)
7     IF(J.GT.MS1.ØR.I.GT.MS2)S(I,J)=0.0
9     READ(40,3)((SC(I,K,J),I=1,K),K=1,M)
3     FØRMAT(10X,6E10.4)
8     FØRMAT(2(10X,E10.4))
6     FØRMAT(A3,3A4)
18    FØRMAT(7E10.3)
19    FØRMAT(10I4)
      PP=P+1
      DØ 20 I=2,RF
20    H(I)=(BC(I)-BC(I-1))/(N(I)-N(I-1))
      H(1)=BC(1)/N(1)
      H(RG)=(BC(RG)-BC(RF))/(NØ-N(RF))
      IF(RG.EQ.1)H(1)=BC(1)/NØ
      DØ 23 J=1,RG
      DR(J)=0.5*H(J)
      DØ 23 I=1,M
23    DH(I,J)=D(I,J)/H(J)
      DØ 60 G=1,M
      DØ 60 I=1,RG
60    TØT(G,I)=SR(G,I)+D(G,I)*BP(I)**2
      DØ 42 K=1,NJ
      I=IJ=1
      IF(RG.EQ.1)GØ TØ 27
      DØ 64 L=1,RF
      IF(K.GT.N(L))I=I+1
54    IF(K.GE.N(L))IJ=IJ+1
27    IF(I.EQ.1)R(K)=K*H(I)
      IF(I.GT.1)R(K)=BC(I-1)+(K-N(I-1))*H(I)
      IF(K.EQ.1)R(K-1)=0.0
      VL(K)=(R(K)**PP-(R(K-1)+DR(I))**PP)/PP
      VR(K)=((R(K)+DR(IJ))**PP-R(K)**PP)/PP
42    RP(K)=(R(K)+DR(IJ))**P
      DØ 11 G=1,M
      DØ 10 K=1,NJ
      I=IJ=1
      IF(RG.EQ.1)GØ TØ 29
      DØ 44 L=1,RF
      IF(K.GT.N(L))I=L+1
44    IF(K.GE.N(L))IJ=L+1
29    JH=G-1
      SLØW(I,K)=SLØW(IJ,K)=0.0
      IF(G.EQ.1)GØ TØ 26
      DØ 62 JK=I,IJ
      DØ 62 J=1,JH
62    SLØW(JK,K)=SLØW(JK,K)+SC(J,G,JK)*FE(J,K)
26    FN(G,K)=-VL(K)*(SLØW(I,K)+SC(G,I))-VR(K)*(SLØW(IJ,K)
     C+SC(G,IJ))
      AN(G,K)=RP(K)*DH(G,IJ)
      IF(K.EQ.1)GØ TØ 28
      CN(G,K)=AN(G,K-1)
      BN(G,K)=AN(G,K)+CN(G,K)+TØT(G,I)*VL(K)+TØT(G,IJ)*VR(K)
      C(K-1)=CN(G,K)/B(K-1)
      B(K)=-BN(G,K)-AN(G,K-1)*C(K-1)
      Z(K)=FN(G,K)-C(K-1)*Z(K-1)
      GØ TØ 10
28    CN(G,1)=DR(1)**P*DH(G,1)
      BN(G,1)=AN(G,1)+CN(G,1)+TØT(G,1)*(VL(1)+VR(1))
      B(1)=CN(G,1)-BN(G,1)
      Z(1)=FN(G,1)
10    FE(G,NJ)=Z(NJ)/B(NJ)
      DØ 11 J=2,NJ
      K=NØ-J
11    FE(G,K)=(Z(K)-FE(G,K+1)*AN(G,K))/B(K)
      WRITE(61,4)ITITLE
4     FØRMAT(1H1,23X,'SEAN SØLUTIØN FØR ',A3,3A4/24X,33('='))
      DØ 12 L=1,NP
      DØ 12 K=1,NJ
      NG=(L-1)*4+1
      NS=L*4
      IF(NS.GT.M)NS=M
      IF(K.EQ.1)WRITE(61,22)(G,G=NG,NS)
12    WRITE(61,21)K, R(K), (FE(G,K),G=NG,NS)
21    FØRMAT(1H ,I3,F8.2,4F15.5)
22    FØRMAT(1HØ,' I PØSITIØN',4(7X,'GRØUP ',I2))
      GØ TØ 24
25    CALL UNEQUIP(40)
      END
```